OXFORD

Oxford Open Materials Science, 2022, 2(1): itac005

https://doi.org/10.1093/oxfmat/itac005
Advance Access Publication Date: 30 June 2022
Review

REVIEW

Materials, electrodes and electrolytes advances for next-generation lithium-based anode-free batteries

Shubhadeep Pal†, Xiaozhe Zhang†, Binson Babu†, Xiaodong Lin, Jiande Wang and Alexandru Vlad ,

Institute of Condensed Matter and Nanosciences, Molecular Chemistry, Materials and Catalysis, Université catholique de Louvain, Louvain-la-Neuve B-1348, Belgium

*Correspondence address. Institute of Condensed Matter and Nanosciences, Molecular Chemistry, Materials and Catalysis, Université catholique de Louvain, Louvain-la-Neuve B-1348, Belgium. Tel: +32 10 47 2555; E-mail: alexandru.vlad@uclouvain.be

†These authors contributed equally to this work.

ABSTRACT

The high volumetric stack energy density (~750 Wh L^{-1}) is a must for grasping the practical application of electric vehicles with more than 100 km per day driving range. Such achievement requires significant advances in state-of-the-art battery technologies. The anode-free, derived from the metal-battery concept, germinates as one of the future potential battery configurations due to the highest, nearly theoretical gravimetric and volumetric energy density. Thus, moving from the graphite-based anode, where lithium is stored as ions, to anode-free cells, wherein lithium is plated as metal, can change the scenario of the electrochemical energy storing devices both in terms of energy density and fundamental mechanism. Although an anode-free battery theoretically provides higher stack energy density than a Li-ion battery, current developments are still underoptimized as these can barely hold for several cycles at room temperature due to the absence of an active lithium reservoir and still severe losses at the anode side. Hence, electrolyte engineering with suitable electrode material choice is highly desirable and extremely challenging in realizing next-generation anode-free batteries. Herein, we summarize the current developments and achievements in the direction of anode-free batteries. Central emphasis is set on electrolyte chemistries that should on one hand allow for high-efficiency initial nucleation, followed by subsequent electrodeposition and electrodissolution of lithium metal, while also forming stable anodic interphases with the high energy cathode materials currently in use. We also prospect for better batteries with higher energy density beyond the present status.

KEY WORDS: anode-free batteries; lithium metal batteries; solid-state batteries; coulombic efficiency; electrolytes; organic materials.

INTRODUCTION

Lithium-ion batteries (LIBs) play a crucial role in human daily life among various energy storage systems [1–6]. With their main application areas gradually shifting from portable electronic devices to electric vehicles, LIBs must meet the ever-increasing demands with an affordable cost, higher energy density, improved safety and extended cycle lifetime. Whereas cost, safety and lifetime are being continuously improved through stepwise materials tuning and engineering approaches, leap forward energy increase, to bring LIBs on par with the energy content of gasoline, rely on disruptive developments in designing cell configurations, electrode/electrolyte material research and their stable interfaces [7–13]. The technical bottleneck set here is the limited intrinsic specific capacity, and thus energy, of the applied materials in LIBs. Disruptive

Submitted: 26 December 2021; **Revised:** 13 May 2022; **Accepted:** 17 June 2022

battery chemistries such as Li–O_2 or Li–S have been proposed over the past decade as challenge-solving solutions [14, 15], but many of these promises turned into disillusion, with practical energy metrics finally below the conventional LIBs [16]. In reality, none of the 'beyond-Li-ion' battery technologies such as single valent (Na/K-ion) or multivalent (Zn/Al/Ca/Mg) metal-ion batteries [17–21], redox flow batteries (RFBs) [22], metal-air batteries [23, 24], dual-ion batteries [25, 26] and hybrid battery-capacitors [27–32] have reached the matured stage yet. By taking into account the aforementioned facts, LIBs will continue to reign the energy storage realm [33].

The current commercially available LIB has a configuration in the form of an anode current collector (CC) | anode material | separator | cathode material | cathode CC, and the lithium salt-based liquid electrolyte infiltrated the porous separator and the electrode material, which provides an ionic path between the electrodes (Fig. 1A). Typically, the commercial LIBs stores/release energy, while charging/discharging, based on the intercalation chemistry at the electrodes [34]. As the main anode material for LIBs, graphite-based electrodes have a high specific capacity and volumetric capacity of ∼372 mAh g^{-1} and ∼841 mAh cm^{-3}, respectively, and operate at a low average potential (150 mV versus Li^+/Li^0), with a high roundtrip energy efficiency, making them the only so far successful commercial anode material [35]. However, the main bottleneck of graphite to meet the ever-increasing demand for small but high-energy-dense batteries is their low volumetric energy density. For instance, the graphite anode with $LiCoO_2$ (LCO) cathode in a pouch cell configuration exhibited a volumetric energy density of 491 Wh L^{-1} [36]. The deployment of graphite composites with silicon increases the gravimetric as well as the volumetric energy density of LIBs, by employing the advantage of the unparalleled theoretical capacity of 4200 mAh g^{-1} (gravimetric) and 9800 mAh cm^{-3} (volumetric) possessed by pure silicon, based on alloy/de-alloy reactions ($Li_{4.4}Si$) [37]. To exemplify, the LIBs consist of Graphite/Si composite anode with LCO cathode exhibiting an increased energy density of ∼600 Wh L^{-1} (volumetric) and ∼300 Wh kg^{-1} (gravimetric) compared with conventional graphite|LCO configuration [∼500 Wh L^{-1} (volumetric) and ∼200 Wh kg^{-1} (gravimetric)] [38]. Similarly, the blending of silicon-rich SiO_x ($x \leq 1$) with graphite has attained much interest in the category of high-energy LIBs [36]. Nevertheless, the huge intrinsic volume change of Si and their derivatives upon lithiation/de-lithiation compared with graphite (≥300% for pure Si and ∼118% for SiO compared with ∼10% for graphite), the graphite/Si or graphite/SiO_x anode undergoes different rates of volume expansion, which induce the failure of the cell upon cycling. Moreover, to date, the battery manufacturers can only incorporate a few amounts of Si or SiO_x (<10 wt%) into the graphite matrixes. The blending of a large amount of Si or SiO_x with graphite requires more optimizations in different parameters, which include the development of compactable polymeric binders to avoid the cracking of the electrodes, functional electrolyte additives to build stable solid electrolyte interfaces (SEIs) that can prevent the electrolyte decomposition over cycling [38, 39]. Lithium metal anode has the potential to drastically reshape the landscape of battery devices due to its high theoretical gravimetric capacity (3862 mAh g^{-1}) and competitive volumetric capacity (2093 mAh cm^{-3}), further supported by the lowest standard redox potential (−3.05 V versus the standard hydrogen electrode [SHE] or 0 V versus Li^+/Li^0) [40–47]. Therefore, by replacing the graphite-based anodes with the lithium metal, which has 10 times more capacity in comparison with the weight of the same graphite, the lithium metal batteries (LMBs) can satisfy the high energy target of 500 Wh kg^{-1} (750 Wh L^{-1}) (Fig. 1B) [48–51].

Unfortunately, the commercialization of LMBs is yet to be realized due to several hurdles [52–54]. One of the main barriers to LMBs is the safety concern induced by the uncontrollable growth of Li dendrites at the Li-metal anode, which results in an internal short circuit, leading to thermal runaway and explosion hazards [55, 56]. Moreover, the high reactivity of Li-metal with the electrolyte exacerbates parasitic reactions leading to electrolyte dry-up [57]. Further, if the Li-metal is not passivated properly, it undergoes continuous irreversible reactions with the electrolyte upon cycling that generates thick SEI layers on the Li-metal surface, which increases the internal resistance of the cell and also consumes an enormous amount of electrolytes that are detrimental to the cell performances [58]. Besides, the low columbic efficiency (CE) during Li, the plating/stripping processes (which leads to shorter cycle life) [59, 60], huge manufacturing costs of fabricating high purity thin Li-metal foils (50 μm) [61, 62] and the difficulty in maintaining environments (dry room conditions, which requires huge investments) for stable Li-metal foil processing (the presence of O_2 and CO_2 reduce the work function of the Li surface by almost 1 eV) [63, 64] are other barriers that prevent LMBs from their large-scale applications.

Considering the various advantages but also the challenges of LMBs and in search of high-energy-density batteries hit another concept of the development of LMBs with zero-excess Li-anode, so-called anode-free LMBs (AFLMBs) or anode-less rechargeable batteries [65, 66]. The AFLMBs have cell configuration in the form of anode CC | separator | cathode material | cathode CC (Fig. 1C), in which there is no anode material (or zero-excess Li anode during the initial discharged state cell assembly), have attracted rapid attention recently, due to its simplified cell structure, low manufacturing cost and can achieve maximum possible energy density [67–71]. Since the anode-free cell design discards the use of any anode materials (e.g. a Li-cation host or a Li metal sheet), the energy is stored/released during charging/discharging relies only on the Li-metal plating/stripping at the anode CC, apart from the Li-ion de-insertion/insertion at the cathode material. Such a design comes along with a series of significant improvements compared with other cells, mainly including the following aspects:

1. the price of AFLMBs is estimated to be significantly lower since no raw electrode materials, solvents, additives and processing is required [72, 73];
2. the costs and challenges in transporting, storing and handling Li-metal sheets are also eliminated;
3. since the conventional anode electrode configuration is now replaced just by a metal foil, the weight and volume of AFLMBs can be significantly reduced, resulting in nearly the highest theoretical possible specific and volumetric energy densities.

The prototype of anode-free cells was initially demonstrated by Neudecker *et al.* [74] in 2000, showing the feasibility of an anode-free Cu/solid lithium electrolyte/LCO thin-film battery. Later, in 2016, Zhang's group [70] reported AFLMBs based on a Cu|$LiFePO_4$ (LFP) cell structure with an extremely high CE (>99.8%) in a liquid electrolyte, opening up new prospects for practical high-energy-density batteries. The significant contributions in this direction were realized by J. Dahn 's group, wherein they have developed a dual-salt lithium difluoro(oxalato)borate (LiDFOB)/$LiBF_4$ with a practical concentration (∼1.2 M) liquid electrolyte for high-performance anode-free lithium-metal pouch cells (80% capacity retention after 90 cycles) [2]. They have also demonstrated

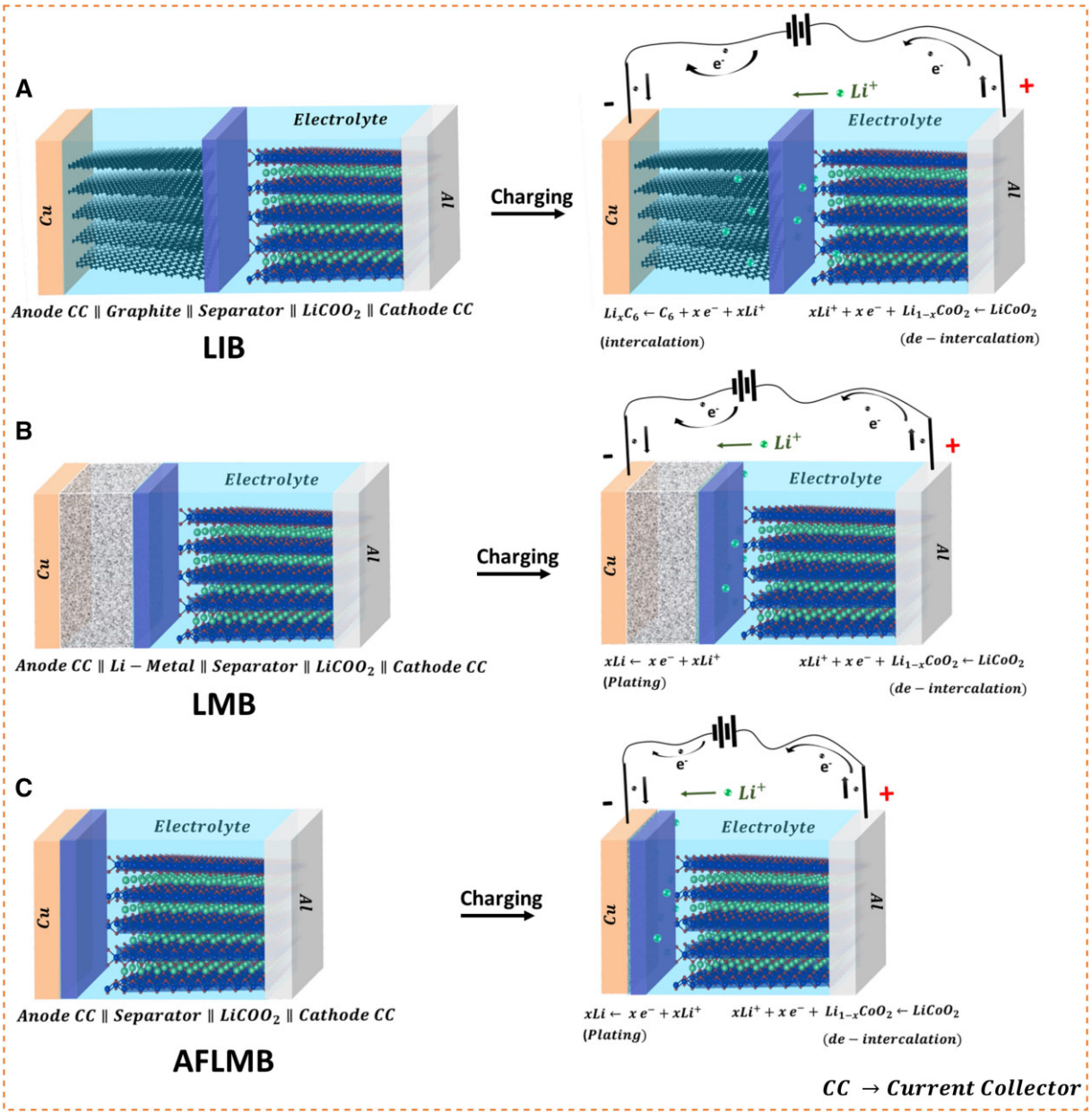

Figure 1: Schematic representation of (**A**) Li-ion battery (LIB), (**B**) Li-metal battery (LMB) and (**C**) anode-free Li-metal battery (AFLMB) and their corresponding operational mechanisms while charging (right side).

AFLMBs with $LiNi_{0.5}Mn_{0.3}Co_{0.2}O_2$ (NMC532) positive electrode assembled with bare copper foil as negative were shown to achieve a stack energy density of 1200 Wh L^{-1}. This is a 60% increase when compared with 700 Wh L^{-1} of conventional LIBs, relying on the same cathode electrode [69].

However, similar to other battery technologies with great energy metric promises, the AFLMB design comes with many technical challenges before any commercial application can be envisioned. For instance, the best performing prototype AFLMBs can sustain 100 cycles, far too low for the current industry targets of more than 2000 cycles lifetime. The main challenge comes from the still hard-to-master Li-metal interface, with the additional challenge of Li-metal nucleation and growth on copper metal foil, and associated first cycle losses.

In this review, we summarize the current work effort strategies of AFLMBs, with the main emphasis on electrolyte chemistries and electrochemical test conditions. Given the limited capacity of commercial cathode materials [75], and that these are the only Li-cation sources in the cell, only if the CE of AFLMBs can be augmented to values close to >99.95%, these may claim practical application value. There have been three main directions approached so far to improve the performance of AFLMBs, including modification of electrolyte, design of CC and optimizing the test protocol. However, relying on exotic structuring techniques or the use of protective films (such as poly(ethylene oxide) [76]) to suppress interface reactions is not yet economically viable. Thus, in this review, we focus primarily on the optimization of test (and especially the cell formation, first cycle) protocols as well as look at how the electrolyte

chemistry can push the boundaries of conventional batteries. So far, AFLMBs developments were relying on inorganic metal oxides cathode materials, but recent advances in the organic battery materials generate hopes for also organic AFLMBs, with the additional advantages of sustainability.

OPTIMIZATION OF TEST PROTOCOLS

One key performance metric of an electrochemical energy storage device is the coulombic efficiency (CE), which measures the reversibility of redox processes at both electrodes. For a lithium metal plating/stripping process, the CE is expressed as

$$CE = \frac{Q_s}{Q_p}, \quad (1)$$

wherein Q_p is the amount of charge passed in the external circuit for a certain amount of Li metal to be plated (electrodeposition) onto a substrate and Q_s is the amount of charge passed in the external circuit to strip (electrodissolution) the respective Li metal amount from the Cu substrate (usually done by fixing the anodic cut-off voltage at +1 V versus Li^+/Li^0). This method of calculating CE remains the most used in the literature due to its simplicity [60].

A lithium-ion battery consists of inorganic cathode material [such as LCO, LFP, $Li[Ni_xMn_yCo_z]O_2$ (NMCxyz, $x+y+z=1$), $LiNi_{0.5}Mn_{1.5}O_4$, etc.), electrolyte with separator and an anode material like graphite or silicon–graphite systems [38, 77–79]. The cathode material is typically deposited on an aluminum foil, whereas the anode material is coated on a copper foil, as these metals are stable at the working anodic and cathodic potentials, respectively. During charging, Li-cations are extracted from the cathode and intercalated in the graphite, forming a C_6Li_x complex (Fig. 1A). The Li is thus stored as an ion which leads systems to run more than 1000 cycles without much loss of active lithium (~90% capacity retention) [80, 81]. The losses take place at both electrodes so that the overall CE is a combination of reversible processes taking place at both, cathode and anode.

An AFLMB is composed of a cathode material (like a LIB), an electrolyte with a separator and a bare copper foil that will act as a negative electrode. For these considerations, it is estimated to provide the highest energy density. During the first charge (formation cycle) of an AFLMB, the Li-cations are released at the cathode and lithium metal is electrodeposited on the copper substrate (Fig. 1C). Considering the highly reactive nature of lithium metal surface toward the electrolyte constituents, it is of paramount importance to know the efficiency of stripping lithium for a particular electrolyte. In fact, for both, LMB and AFLMB, the efficiency of the lithium metal plating and stripping is accounted as the main limiting factor on the cycling stability. Thus, the formation of a stable SEI layer to block further electrolyte decomposition is essential to any LMB or AFLMB [82]. A system with constant CE over cycles is expected to have a 10-fold increase in cycle number lifetime if an increase of CE from 90% to 99% is attained, as estimated by Nanda *et al.* [65]. However, in their work, a constant CE is assumed from the beginning of cycling which is often far from reality but can provide a reasonable estimation of the lifetime of an LMB and AFLMB. In most cases, CE is stabilized after a few initial cycles, and depending on SEI stability, it can either reach values above 99.5% or stabilize below 99%. For example, Yu *et al.* [83] have reported a designed single solvent (fluorinated 1,4-dimethoxylbutane) with 1 M lithium bis(fluorosulfonyl)imide (LiFSI) attained fast passivation and reached a CE of ~99.52% within five cycles, while an electrolyte composition made of 0.3 M lithium bis(trifluoromethanesulfonyl)imide (LiTFSI) with fluoromethane (CH_3F, FM)-based liquefied gas electrolyte was shown to achieve an average CE of 98.6% after 100 cycles [84]. The CE has a huge impact on the cycle lifetime since a CE of >99.5% can provide 100 cycles with 80% capacity retention, whereas a CE < 99% can only sustain 20 cycles if a limited Li source is available [59, 70]. Thus, based on the electrolyte composition and its ability to efficiently passivate Li-metal surface, the number of cycles required to get a stable CE also varies, leading to continuous increment of discharge capacity until reaching a stable regime.

Recently, many efforts have been focused on attaining CE of >99% of lithium metal yet whose distinctive bulk mechanical properties are often neglected, still expected to have a major influence on the performances of AFLMB [65]. Although various strategies have been applied, such as CC modification or protective coatings on the CC, none of the above brings the fundamental reason for cell failure [85]. The inhomogeneity and high dynamic nature of the Li-metal surface, especially while plating and stripping, makes it difficult to understand the basic cause of the poor performance of cells qualitatively as well as quantitatively [86]. Nevertheless, there is a growing consensus that the mechanical properties of Li have a strong influence on dendrite formation, which results in SEI layer breaking and separator penetration which finally causes short-circuit and cell failure [87, 88]. It has been found that the application of mechanical stress or pressure can effectively suppress the dendrite growth [89–91]. The model proposed by Monroe and Newman [92] suggests that the distribution of elastic stresses at the electrode/electrolyte interface drives the dendrite growth and can be suppressed by the utilization of solid polymer electrolytes (SPEs) having shear modulus greater than two times that of Li. This study shines light in the direction of the usage of solid or polymer electrolytes in batteries, which can provide sufficient compression on the anode surface and may induce Li-deformation (create flat Li-morphology), owing to the low yield strength and large plasticity of lithium [88, 93]. Louli *et al.* [94] have shown an enhanced cycling performance and lithium plating efficiency of (NMC532|Cu) anode-free cells, while increasing the initial average pressure from 75 to 2200 kPa. In addition to this, they have also observed that the cell cycling performance is not equally benefited under increased pressure when different solvents are involved, rather it also depends on the physical properties of electrolytes. Moreover, owing to the relatively low melting point (453 K) of Li-metal, the mechanical properties are strongly dependent on the temperature and strain rates [95] and also due to the low activation energy for self-diffusion of solid Li, the dislocation creep (power-law creep) is found to be dominant at room temperature [96, 97].

Dasgupta's research team has conducted comprehensive studies related to the mechanical response of Li over a wide range of temperature and strain rates [87]. They observed that the strain hardening only occurs at high strain rates and low temperatures, which illustrates that the power-law creep is the significant deformation mechanism in Li-metal over a wide range of current densities and battery-operating conditions. So far, researchers have empirically optimized the best working current density to find the optimal CE without emphasizing the reason behind it. Here, in the above work, an electrochemical–mechanical relationship has been described between the strain rate and current density, indicating that dislocation creep is controlled by the current density, which will impact the Li-morphology and ultimately influence the CE. They have also

shown that the creep stress decreases at high temperature, which facilitates the plastic deformation quality of the Li metal, and produces planar morphology as Li follows power-law creep dislocation mechanisms [87].

By considering the above results and the other studies [98, 99], showing an improved effect of temperature on the cycling stability of lithium metal coin cells, Genovese *et al.* [100] have proposed a unique protocol named 'Hot Formation' for NMC 532 | Cu anode-free lithium metal pouch cells, with a LiDFOB/$LiBF_4$ dual salt electrolyte composition. In this protocol, before cycling the anode-free pouch cell at low temperature, it is subjected to two initial high temperature (40°C) cycles (C/10 charge C/2 discharge). It is found that these two initial high-temperature cycles have a profound effect on the cycling stability of anode-free cells, showing improved capacity retention of 80% for 60 cycles compared with 18 cycles without hot formation at low-pressure (Fig. 2A). This improved cell performance is attributed to the favorable lithium morphology formation due to the increased creep dissolution at higher temperatures and is also attributed to the increased gas (CO_2) generation which is found to be a better SEI film-forming additive in the lithium metal cells [101]. In addition, a high stacking pressure (1200 KPa) further improves the cell performance (showing 85% capacity retention at 100 cycles after the hot formation cycle), by taking into account the improvement in the seeded lithium nucleation processes under high pressure [102, 103]. After the careful optimization of the current density used for the formation cycle and subsequent cycling, a performant and stable AFLMB has been attained in Dahn's laboratory. Lithium-ion cells or half-cells (in particular in laboratory testing conditions) are typically cycled at equal charge and discharge current and there is no particular reason to apply different rates between charge and discharge current (yet, this is being done in practice). Louli *et al.* [104] have found that asymmetric charge-discharge currents can influence the cell cycling behavior of AFLMB. Three different conditions have been tested such as symmetric charge-discharge, asymmetric fast charge (AFC) and asymmetric slow charge (ASC) (Fig. 2B). It has been found that the asymmetric protocols with the charge being slower than the discharge rate are better for high-performance anode-free cells (Fig. 2C). As it is quite intuitive that the smooth SEI layer formation can be attained only during slow charging. At a high charge current density (i.e. corresponding to lithium plating at the anode), lithium deposition is uneven at boundaries or surfaces due to the generation of a concentration gradient or non-uniform pressure development, leading to the formation of porous or dendritic structures. On the other hand, asymmetric fast discharge was found to mitigate the loss of active lithium, the so-called dead

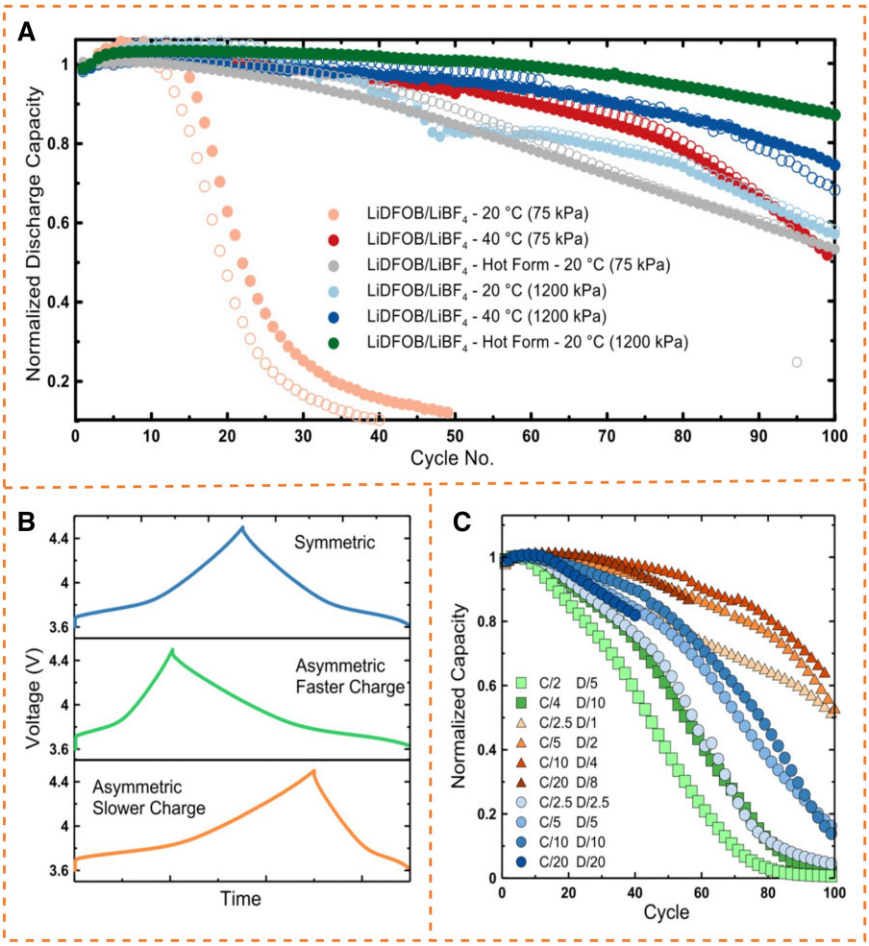

Figure 2: (**A**) Cycling stability of NMC 532||Cu anode-free cell under low (75 kPa) and high (1200 kPa) pressure at 20°C and 40°C without hot formation as well as at 20°C with a hot (40°C) formation protocol. Reproduced from Ref [100]. (**B**) Voltage profile showing different charge–discharge rate tests: symmetric charge–discharge, AFC and ASC. (**C**) Cycling stability of NMC 532||Cu anode-free cell at different charge–discharge protocols: symmetric charge–discharge (blue color), AFC (green color) and ASC (orange color). The cells were cycled in the voltage range of 3.6–4.5 V at 40°C under low pressure (170 kPa) in the electrolyte formulation of 0.6 M LiDFOB + 0.6 M LiBF4 in FEC:DEC (1:2). Reproduced from Ref. [104].

lithium. For instance, after a fast discharge step (i.e. lithium deposit dissolution), a uniform surface is left on the anode CC, which was suggested to favor the deposition at the next step. Thus, a combination of slower charging and faster discharging, in particular, 2.5 times faster discharging than charging, minimizes the lithium inventory loss while plating and stripping, which seems to be more advantageous. Hence, by maintaining this charge–discharge ratio, faster charging should be possible for AFLMBs without significantly compromising their performance. Along with this technique, creating and making use of a lithium reservoir [e.g. by limiting the discharge capacity or the depth of discharge (DoD)] has been seen to be beneficial for the long cycle life of AFLMBs. Therefore, by implementing an intermittent high DoD protocol, it is possible to extend the lifetime of AFLMBs while maintaining the ability to occasionally provide high energy density.

MODIFICATION OF ELECTROLYTE

Liquid electrolyte

The chemistry of the electrolyte has probably the most important influence on the stability of AFLMBs, as the lithium metal nucleation and possible dendrite growth, as well as the quality of the SEI layer and ultimately the CE are all intimately dependent on this [3, 105–107]. As a direct product of electrolyte decomposition, SEI plays an essential role in the electrochemical performance of AFLMBs. An ideal SEI should be an electronic insulator as well as dense and compact (to thus completely suppress undesirable side reactions between the electrolyte and metallic lithium), while at the same time having a high ionic conductivity. Therefore, electrolyte modification strategies for better AFLMBs are being discussed in this section, including the choice of solvents, salts combination and use of SEI film-forming additives.

Solvent chemistry

Carbonates [ethylene carbonate (EC), propylene carbonate (PC), dimethyl carbonate (DMC), ethyl methyl carbonate (EMC), diethyl carbonate (DEC), etc.] and ethers [dimethoxyethane (DME), 1,2-dioxolane (DOL), diglyme, etc.] are the two main classes of organic solvents used for battery electrolytes [108, 109]. Among these, the most conventional, also applied in the commercial LIBs, are the carbonate-based electrolyte with 1.2 M $LiPF_6$ as salt and a variety of additives [110, 111]. However, carbonates have high reactivity with lithium metal electrodes, greatly restricting their application in AFLMBs [110, 112, 113]. In contrast, ether-based electrolytes have higher compatibility with lithium metal, due to better passivation of the lithium metal surface [2, 114, 115]. However, the low anodic stability of ether-based solvents hinders their practical application, especially when targeting high potential cathode materials (>4 V versus Li^+/Li^0). At the same time, the carbonate-based electrolytes can be used up to >5 V (versus Li^+/Li^0) due to their higher electrochemical stability window and also film-forming ability at the cathode surface [116].

To enable these both classes of solvents to be compatible with 4V—class cathodes, and also to stabilize the Li-metal surface (and thus eventually suitable for AFLMBs), high concentration electrolytes (HCEs) have been suggested and tested as a feasible solution [114, 117]. Unlike the conventional electrolyte used in LIBs with a salt concentration of 1 – 1.5 M, HCEs have concentrations of more than 3 M, depending on the salt solubility in the given solvent. The major change of HCEs when compared with diluted systems is that beyond a certain concentration threshold, all solvent molecules are being located in the primary solvation shell of the Li-cations, thus no (or a negligible amount of) free solvent molecules are available (Fig. 3A). Being strongly bound, the solvent molecules are kinetically and thermodynamically stabilized, with thus anions being preferentially decomposed and leading to anion-derived SEI films. The function of anion chemistry, the SEI composition may be consequently enriched by inorganic species such as LiF and Li_2O, known as more suitable than organic or polymeric species formed by the decomposition of solvents. The LiF-rich SEI layers are more suitable than the solvent-derived SEI layers, thus higher salt concentration can fundamentally change the SEI composition to improve the anode stability and achieve a higher CE [118, 119]. Furthermore, an inorganic-rich SEI can effectively inhibit the formation of lithium dendrites and guide the two-dimensional growth of lithium metal [112, 120–124].

Qian *et al.* [112] have reported the use of ether-based HCEs in lithium metal anodes and have confirmed the good compatibility between lithium metal and 4 M LiFSI in DME, which exhibits high-rate cycling stability with a high CE (up to 99.1%) without dendrite growth. The utilization of this HCE formulation also enables the Cu|lithium cell to cycle more than 1000 cycles with an average CE of 98.4% at a current density of 4 mA cm^{-2}. This improved performance is ascribed to the relatively high electrolyte reductive stability due to low solvent content, high compact SEI layer induced by anion decomposition and increased Li-ion concentration (enables high-rate Li plating/stripping with high CE) of HCEs compared with the diluted electrolytes. Further, this electrolyte composition was used in a Cu|LFP AFLMBs, which can maintain 60% capacity retention after 50 cycles with an average CE of more than 99% (Fig. 3B), at a current density of 0.2 mA cm^{-2} and an initial charge capacity of 1.7 mAh cm^{-2} (corresponding to a specific capacity of 148 mAh g^{-1}) [113].

HCEs based on carbonate solvents have also been found to improve the cycling performance of AFLMBs as Nilsson *et al.* [114] demonstrated. A Cu | Solupor | LFP cell (Solupor 3P07A single-layer polyethylene membranes used as separator here as it is easily wet by 6 PC and EC-DEC and instantly wet by DOL-DME and also acts as a barrier toward dendrite growth) in a LiTFSI-6EC [LiTFSI: EC = 1:6, molar ratio (MR)] as electrolyte was constructed and shown to maintain 41% capacity retention after 30 cycles, at a current density of 1.0 mA cm^{-2} after the initial cycle at 0.1 mA cm^{-2}, with a capacity density of 3.5 mAh cm^{-2} (Fig. 3C). Although these HCEs can improve the performance of carbonate-based and ether-based electrolytes, they still suffer from many disadvantages including high cost, high viscosity, poor ability to wet polymer separator and low ionic conductivity, which will affect their application in AFLMBs [127].

Recently, a new concept of localized high-concentration electrolytes (LHCEs) has been introduced and attracted tremendous attention due to in particular potentially low costs of such systems [128]. By introducing a low-polarity diluent in HCEs, the concentration and viscosity are decreased without changing the Li^+ solvation structure. In conventional diluent electrolytes, Li^+ is mainly solvated as solvent-separated ion pairs (SSIPs) structure since there are sufficient solvent molecules (Fig. 3A1). Instead, a large fraction of anions coordinates with Li^+ ion through contact ion pairs (CIPs, anion coordinating to a single Li^+ cation) or cation–anion aggregates (AGGs, anion coordinating to two or more Li^+ cations) in the HCEs and LHCEs as shown in Fig. 3A2 and A3. Thus, the LHCEs can inherit the excellent performance of HCEs, but greatly reduce the salts concentration of the entirety electrolyte.

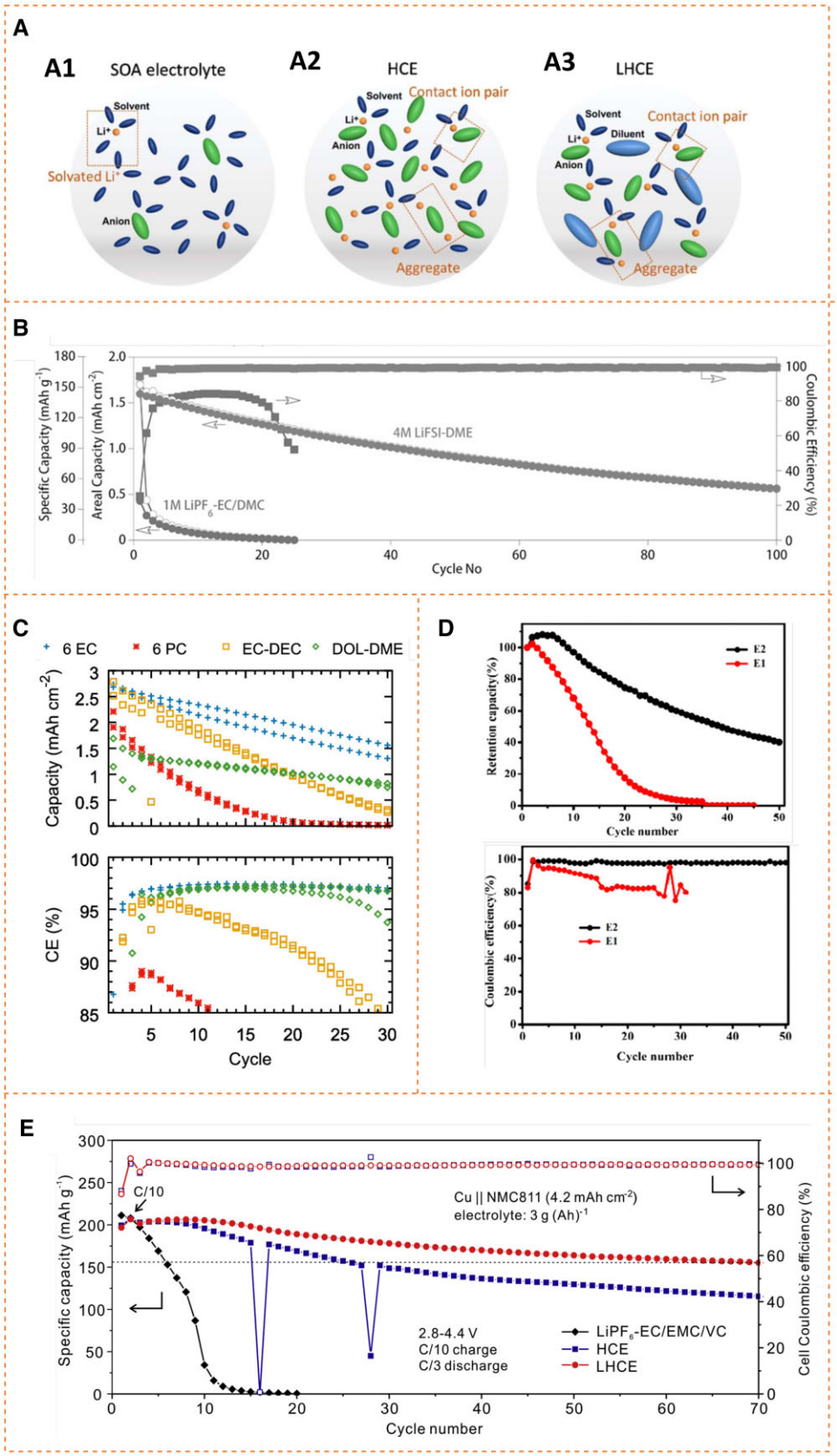

Figure 3: (**A**) Schematic of electrolyte structures of (**A1**) state-of-the-art (SOA) electrolyte, (**A2**) high-concentration electrolyte (HCE) and (**A3**) LHCE. Reproduced from Ref. [117]. (**B**) Electrochemical performance of Cu||LFP AFLMB with 1-M $LiPF_6$-EC/DMC and 4-M LiFSI-DME electrolyte formulations. Reproduced from Ref. [113]. (**C**) Discharge capacity (above) and CE (below) for Cu||Solupor||LFP cells. Reproduced from Ref. [114]. (**D**) Comparison of retention capacity (%) (above) and CE (below) of Cu||NMC111 AFLMB using E1 ($LiPF_6$ in EC/DEC 1:1 v/v ratio) and E2 [$LiPF_6$ (EC/DEC) 1:1 v/v ratio, diluted by 50% FEC] electrolytes. Reproduced from Ref. [125]. (**E**) Cycling performances of Cu||NMC811 cells in different electrolytes. Reproduced from Ref. [126].

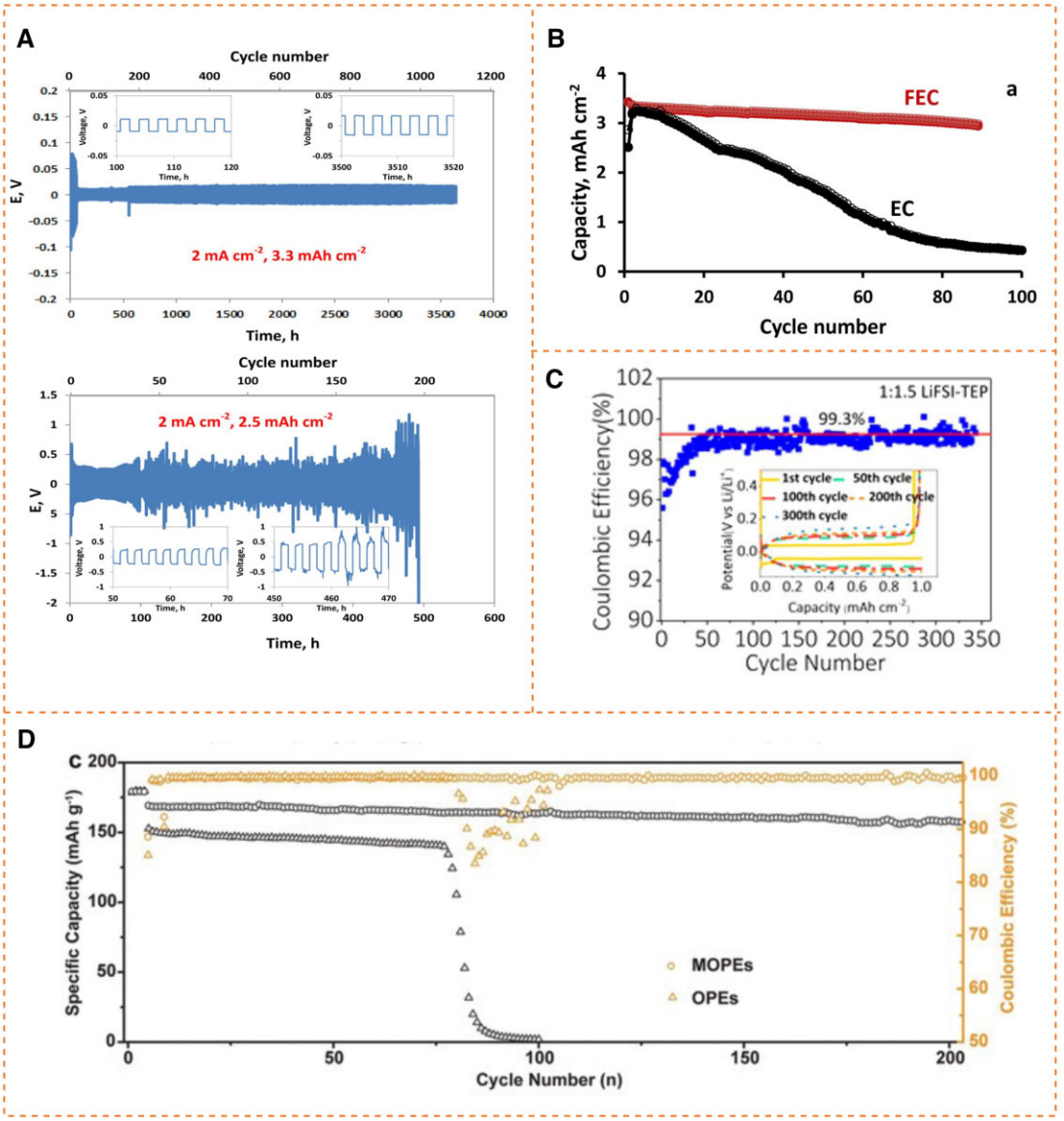

Figure 4: (**A**) Galvanostatic cycling profile for symmetric Li||Li cells in 1 M $LiPF_6$/FEC/DMC (above) and 1 M $LiPF_6$/EC/DMC (below) electrolytes cycled with a current density of 2 mA cm^{-2}. (**B**) Compare the cycling stability of Li||NMC cells in FEC- and EC-based electrolytes at a current density of 0.5 mAcm^{-2}. Reproduced from Ref. [130]. (**C**) CE profile of Li metal plating/stripping in the Li||Cu cell cycled at a current density of 0.1 mA cm^{-2} in the first cycle and then 0.2 mA cm^{-2} in MR of LiFSI:TEP is 1:1.5 electrolyte. Inset: Voltage profile of the Li||Cu cell at selected cycles. Reproduced from Ref. [139]. (**D**) Cycling performance of Li|MOPE|NCM622 cell. Reproduced from Ref. [140].

Hagos *et al.* [125] use fluoroethylene carbonate (FEC) diluent (but most certainly also acting as an SEI film-forming additive) in a 2-M $LiPF_6$ in EC/DEC (v/v: 1/1) electrolyte, which allowed a Cu|$LiNi_{1/3}Mn_{1/3}Co_{1/3}O_2$ AFLMB (NMC111 cathode with a mass loading of ∼2 mA h cm^{-2}) to cycle with an average CE of 97.8% and 40% retention capacity after 50 cycles at a current density of 0.2 mA cm^{-2} (Fig. 3D). Compared with the HCEs, AFLMBs with LHCEs show the same stable cycling performance but lower viscosity and thus higher ionic conductivity. Ren *et al.* [126] investigated LHCEs based on ether solvent, employing an electrolyte consisting of LiFSI salt in DME within a MR of 1:1.2 (corresponding to 8 M), with the addition of 1,1,2,2-tetrafluoroethyl-2,2,3,3-tetrafluoropropyl ether (TTE) as the diluent. The final molar composition ratio was 1LiFSI–1.2DME–3TTE and was found to sustain stable cycling over 70 cycles with a capacity retention of 77% in a Cu|NMC811 ($LiNi_{0.8}Mn_{0.1}Co_{0.1}O_2$) AFLMB configuration (Fig. 3E).

The modification of the solvent chemistry and composition can also affect the stability of the lithium striping and plating process. It has been shown that LiF-rich SEI shows higher toughness than organic-rich SEI [129]. Therefore, the introduction of fluorine elements into the solvent structure can result in the generation of higher amounts of LiF upon the decomposition of solvent molecules on the anode surface. Markevich *et al.* [130] have tested symmetrical lithium metal cells at a high current density (2 mA cm^{-2}) and high areal capacity (3.3 mAh cm^{-2}) with 1 M $LiPF_6$ in EC/DMC and 1 M $LiPF_6$ in FEC/DMC electrolytes and found that for the FEC containing cells, cycling over more than 1000 cycles was possible (Fig. 4A). Based on this electrolyte formulation, Li|$LiNi_{0.6}Co_{0.2}Mn_{0.2}O_2$ (NMC622) cell with high mass loading cathode (3.3 mAh cm^{-2}) have shown capacity retention of ∼88% over 90 cycles, far higher than for the EC-based electrolyte (∼10% after 90 cycles, Fig. 4B). The better lithium metal compatibility with

FEC-based electrolytes was attributed to the formation of a stable and LiF-enriched SEI.

Generally, cyclic carbonate such as EC and ether-based electrolytes can form stable SEI. Still, due to its intrinsic flammability, abusive battery operation or failure can lead to fire or even explosion if proper protection is not adopted. Recently, organic phosphates electrolytes (OPEs) have attracted considerable attention due to their intrinsic fire-retardant ability, low cost and suitable physicochemical properties (high dielectric constant and high solubility in various salts), which could intrinsically eliminate fire hazards and improve battery safety [131, 132]. However, the main drawback of OPEs is that most linear chain phosphates do not form a stable SEI film and are thus not compatible with graphite, silicon or lithium metal anodes when applied as electrolyte solvents at low salt concentrations [133–136].

To improve the performance of OPEs, Zheng *et al.* [137] introduced the fluorinated strategy on phosphates groups by fusing the cyclic carbonates (form stable SEI) with organic phosphates (that can trap hydrogen radicals and prevent combustion). They have synthesized a five-membered fluorinated cyclic phosphate called 2-(2,2,2-trifluoroethoxy)-1,3,2-dioxaphospholane 2-oxide (TFEP) and found an enhancement in the anodic stability, as well as significantly improve the SEI stability at low potential working electrodes. The designed TFEP solvent molecule thus integrates a phosphate group (for nonflammability) and a trifluoromethyl group to engender an F-rich SEI [137, 138].

It is found that the stability of non-flammable phosphate electrolytes is improved by adjusting the MR of Li salt to solvent [132]. Xiao *et al.* [139] reported the use of LiFSI-triethyl phosphate (LiFSI-TEP, MR =1:1.5) electrolyte in Li|Cu cells provides a stable lithium plating/stripping up to 350 cycles with a high CE of 99.3% (Fig. 4C). Tan *et al.* [140] modify the OPEs with a nitriding interface strategy via lithium nitrate modified organic phosphate electrolytes (MOPEs). The synthesized MOPEs consist of 1 M LiTFSI in TEP with 2% vinylene carbonate (VC) and 5% lithium nitrate ($LiNO_3$) as the additive. The use of MOPEs in Li| NMC622 showed a capacity retention of 94.7% even after 200 cycles (Fig. 4D). This improved cell performance is ascribed to the inorganic-rich SEI formation in the lithium metal surface, due to the decomposition of $LiNO_3$.

Even though many advances are happening in the realm of phosphate-based electrolytes, no studies have been conducted so far on the utilization of these electrolytes in AFLMBs. The continuous improvement of lithium deposition efficiency and the intrinsic flame-retardant advantages makes this chemistry one of the preferred choices for AFLMBs electrolytes.

Salt and anion chemistry

Salt, particularly anion chemistry, is another important part of the electrolyte since it directly participates in SEI formation. The most common salts mainly rely on PF_6^-, FSI^- and $TFSI^-$ anion chemistries. The $LiPF_6$ is the most widely used salt, largely applied in commercial cells, due to its proven electrochemical and physico-chemical properties and low costs. It induces the formation of high electronic resistive LiF in the SEI layer (which increases the impedance of the cell) and is also sensitive to moisture [113, 115]. LiFSI and LiTFSI salts can also form a LiF-rich SEI to passivate the lithium metal surface and improve the compatibility, but the costs remain high. Moreover, these salt chemistries are known to corrode the aluminum CC at high voltages (>3.7 V versus Li^+/Li^0) [141]. Therefore, it has become important to develop novel salt chemistries, cope with both drawbacks and find optimal multi-salts combinations in electrolytes for better performance of AFLMBs.

Dahn *et al.* [2, 69] have reported a dual-salt carbonate-based electrolyte with 1 M LiDFOB and 0.2 M lithium tetrafluoroborate ($LiBF_4$) in FEC:DEC (volume ratio of 1:2), in cell pairing a single-crystal $LiNi_{0.5}Mn_{0.3}Co_{0.2}O_2$ (NMC532, 94% active, 16 mg cm^{-2}, 3.5 g cm^{-3}) positive electrode with a bare copper foils CC. The cell, cycled under 40°C, C/5 charge and C/2 discharge, between 3.6 and 4.5 V conditions, maintained 80% of the initial capacity over 90 cycles (Fig. 5A). It is worth mentioning that such a significant advance for the AFLMBs concept is achieved in a practical large-area pouch cell under lean electrolyte conditions, with an electrolyte amount to capacity ratio of 2 g Ah^{-1}. The remarkable AFLMBs performance in this dual-salts electrolyte was attributed to the robust SEI formation with an optimal ratio of inorganic and organic components. The decomposition of LiDFOB is rich in organic boronated and fluorinated components and the $LiBF_4$ is prone to decompose to inorganic components such as LiF. Although such a dual-salt electrolyte allowed for a significant breakthrough in extending the cycle lifetime of AFLMBs, the continuous consumption of LiDFOB and $LiBF_4$ during cycling remains a central issue to be solved. Dahn's group further reported another dual salt electrolyte with optimized salt composition and concentration in 2020 [69]. A high-concentration dual-salt electrolyte made of 2 M LiDFOB and 1.4 M $LiBF_4$ in FEC/DEC (volume ratio of 1/2) was found to improve the cycle lifetime of NMC532|Cu pouch cells of up to 200 cycles with 80% capacity retention. This work attained one of the highest energy density AFLMBs with the longest lifetime (Fig. 5B). It was suggested that the optimal ratio of LiDFOB to $LiBF_4$ promotes the formation of a smooth mosaic of tightly packed lithium columns, assigned as beneficial to the uniform deposition and high CE of lithium deposits. However, the lithium morphology is prone to degradation due to continuous salt consumption and upon major/significant salt exhaustion, the cell fails to cycle further.

Dual salts systems can also be applied with ether-based electrolytes as Alvarado *et al.* [127] reported with a 2.3-M LiTFSI and 4.6-M LiFSI salt system in DME. The NCM622|Cu coin cell using this electrolyte composition have a residual capacity of 90.9 mAh g^{-1} and CE of 98.6% after 54 cycles, at C/10 during the charge cycle and C/3 during the discharge state. While only 54.8 mAh g^{-1} and a CE of 97.4% for 4.6-M LiFSI in DME, and quickly fades with no remaining capacity for 1.0-M $LiPF_6$ in EC/EMC 3:7 after 30 cycles (Fig. 5C). It is worth noting that a similar concentration single salt electrolyte of 6.9 M LiFSI in DME shows a significantly faster capacity fade than the 6.9 M dual salt electrolyte in Fig. 5C. Although the HCEs have been confirmed to improve the high-voltage stability of ether-based electrolytes in the previous paragraph, the synergy effect of FSI^- and $TFSI^-$ plays a more crucial role in the batteries cycling stability here. Based on the modeling predicted by the authors, the $TFSI^-$ can slow the reaction rate of FSI^- decomposition by absorbing electrons from the metal, leading to a slowly aggregate of LiF and other LiFSI reduction products during the SEI forming process in dual salts electrolyte, as opposed to rapid and excessive LiFSI reduction in the single salt HCEs. Such a unique anion decomposition mechanism in dual salts electrolyte results formed a more uniform and robust SEI, which allows the lithium stable deposition.

The detail of the deposited Li metal on Cu foil (Li|Cu coin cell) was further analyzed by cryogenic-focused ion beam (cryo-FIB) and SEM imaging (Fig. 5D). A significant difference in the electroplated Li-metal morphology is observed between these

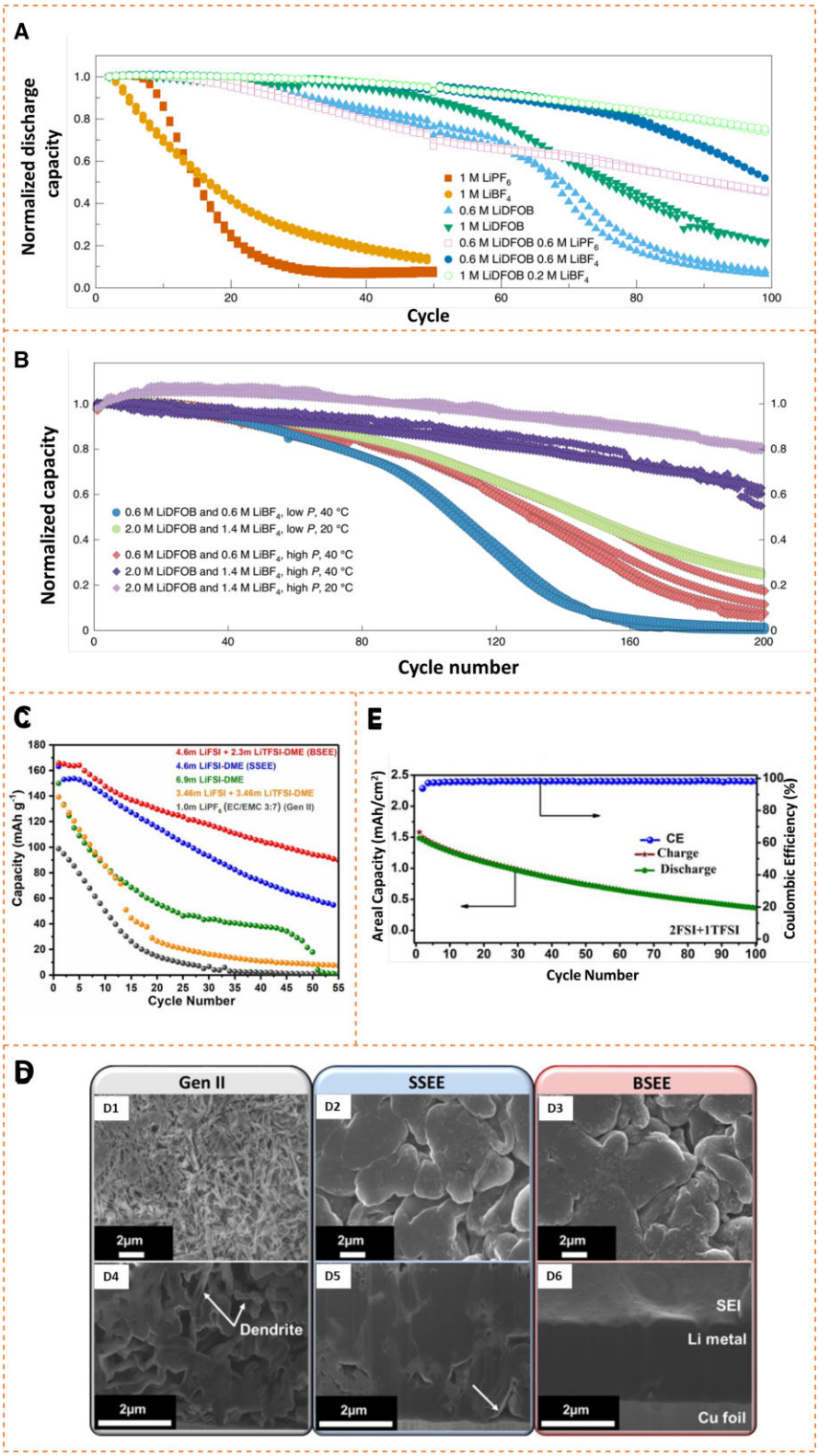

Figure 5: (**A**) Capacity retention for NMC532||Cu anode-free pouch cells using electrolytes with different lithium salts. Cells were cycled at 40°C, C/5 charge and C/2 discharge, between 3.6 and 4.5 V, with an areal capacity was about 2.4 mAh cm^{-2} and a total pouch cell capacity was about 250 mAh. Reproduced from Ref. [2]. (**B**) Normalized capacity versus cycle number for NMC532||Cu anode-free pouch cells cycled under high pressure at 20°C, C/5 charge and C/2 discharge, between 3.6 and 4.5 V, the areal capacity of the positive electrode was about 3.1 mAh cm^{-2}. Reproduced from Ref. [69]. (**C**) Electrochemical testing of NMC622||Cu coin cells with various electrolyte formulations. Plated at C/10 and stripped at C/3. Reproduced from Ref. [127]. (**D**) Top-view SEM images of the initial morphology of plated lithium and their corresponding Cryo-FIB cross-sectional cuts when cycled in (**D1, D4**) 1.0 M $LiPF_6$ in EC/EMC 3:7(Gen II); (**D2, D5**) 4.6 M LiFSI in DME (SSEE) and (**D3, D6**) 4.6 M LiFSI + 2.3 M LiTFSI in DME (BSEE). Reproduced from Ref. [127]. (**E**) Capacity retention and CE of LFP||Cu coin cells cycled in the 2-M LiFSI + 1-M LiTFSI in DME/DOL dual salt electrolyte between 3.0 and 3.8 V versus Li/Li^+, at current densities of 0.2 mA cm^{-2}. Reproduced from Ref. [142].

three electrolytes. In the single salt carbonate-based electrolyte [1.0 M $LiPF_6$ in EC/EMC 3:7 (Gen II)] used as a baseline reference, the lithium grows as dendrites, consistent with most previous reports [143]. In the 4.6 M LiFSI in DME single salt ether electrolyte (SSEE), the high salt concentration is beneficial to forming a microporous, closely packed nodular Li metal morphology. However, small pores are still present close to the Cu interface, indicating inhomogeneities in the areal current density distribution in the single-salt system. In contrast, the bisalt ether electrolyte ('BSEE', 4.6 m LiFSI + 2.3 m LiTFSI in DME) allows for much uniform, dense and conformal lithium deposition without dendrites.

According to the same rationale, yet relying on a lower concentration electrolyte, Beyene *et al.* [142] used a 2-M LiFSI with 1-M LiTFSI dual-salt system in DME/DOL (vol. 1:1) solvents. A Cu|LFP AFLMB with such electrolyte was able to sustain stable cycling for 100 cycles with a high CE of 98.9% and retain more than 50% of its initial capacity after 50 cycles at an areal current density of 0.2 mA cm^{-2} (Fig. 5E). According to the authors, the limited amount of LiTFSI added to the dual salts system increases the conductivity of the electrolyte to 7.91 mS cm^{-1}, higher than the 2.65 mS cm^{-1} of 3 M LiTFSI in DOL/DME and 5.26 mS cm^{-1} of 3 M LiFSI in DOL/DME single system electrolytes. Meanwhile, the less stable FSI^- tends to decompose and conduce to form a more compact SEI layer. The improved electrolyte conductivity and the formation of good SEI synergistically improved cycle life and CE of the AFLMBs.

Electrolyte additives

Compared with the modification of solvents and salts, adding additives to improve the performance of electrolytes in lithium metal anode is considered a more economical and simple way. There are no clear definitions as to what concerns the amount of additive to be considered as co-solvent or co-salt in the electrolyte. Thus, we define components in the electrolyte with a volume or mass ratio lower than 10% as additives, thus distinguishing these from dual-salt or dual-solvent systems discussed in previous chapters [70, 144–147].

The electrolyte additives can be grouped according to their main function, which may include the most common flame-retardancy, film-formation, self-healing, redox mediation and the self-discharge limitation [70, 148–152]. Because most of the capacity fade occurs in AFLMBs attributed to the uneven deposition of lithium metal, thus, here we have summarized and discussed additives below through the improvement of the morphology of the deposited lithium. Although certain additives can have functions simultaneously, we focus mainly on the film role and analyze the mechanism in detail.

Zhang *et al.* [153] found that rubidium fluoride (RbF) additive can effectively inhibit lithium dendrite growth. Due to higher electropositive properties, the authors suggested that Rb^+ are attached to the prominent dendrite tips, forming an electrostatic shield at the surface, thus lithium depositing evenly to form a smooth and compact morphology (Fig. 6A). As a result, a Li|Li symmetrical cell could cycle over 1000 cycles with CE above 90% in 1 M $LiPF_6$ in EC/DMC (vol. 1/1) electrolyte with 0.05 M RbF as additive. Choi *et al.* [154] used the ionic liquid additives namely 1-dodecyl-1-methylpyrrolidinium $(Pyr1(12)^+)$ bis(fluorosulfonyl)imide (FSI^-) to improve the lithium deposition. The $Pyr1(12)^+$ cation was also suggested to repel the Li-ions flux via electrostatic repulsion since it can maintain a positive polarity during charging, thus alleviating Li dendritic growth (Fig. 6B1) [150]. Moreover, the author supported that the nonpolar aliphatic chain attached to the pyrrolidinium can provide a 'lithiophobic' effect, which can further guide lithium deposition to avoid the formation of lithium dendrites. It is worth mentioning that the FSI^- anions can help to form an inorganic-rich SEI to suppress interface reactions. Thus, through the synergistic effect of anion and cation in the electrolyte, the LFP|Li coin cell sustained 74.6% capacity retention over 500 cycles at a current density of 0.8 mA cm^{-2} (Fig. 6B2). A similar strategy was proposed by Sahalie *et al.* [155]. They used potassium nitrate (KNO_3) as an additive. They found improved cycling stability of Cu|NMC AFLMBs, with 40% of the initial capacity retention after 50 cycles in the 1-M $LiPF_6$ EC/DEC (1:1 v/v) electrolyte, while only 40% initial capacity retention after 15 cycles in 1-M $LiPF_6$ EC/DEC (1:1 v/v) without additives. According to the authors, K-ions were also suggested to have an electrostatic shielding effect on Li^+, resulting in the formation of a uniform and dense lithium deposit morphology (Fig. 6C).

Tuning the SEI composition and properties by using additives is another method to stabilize the lithium deposition process. The nitrate (NO_3^-) anions have been shown to play an important role in the SEI regulation//formation since the decomposition was confirmed to generate nitrogen-containing species such as Li_3N, which possesses a high Li^+ ion conductivity ($>10^{-4}$ S cm^{-1}) and can thus significantly decrease the interfacial resistance [140, 156, 157]. However, the drawback of $LiNO_3$ is its low solubility and compatibility with the carbonate solvent systems. To circumvent this issue, Lucht *et al.* [158] used triethylphosphate (TEP) as a co-solvent in EC/DMC electrolyte (ratio of TEP:EC:DMC is 8.4:8.4:83.2, by volume), attaining a solubility of 0.2-M $LiNO_3$ in the nominal formulation of 1 M LiDFOB in EC/DMC. The CE of the assembled Cu|LFP anode-free coin cell with this electrolyte composition reached 99% after 15 cycles, with 80% loss of the initial capacity after 65 cycles (Fig. 7A) [158]. The same group also used 5% (by mass) VC as additives in 1.2 M $LiPF_6$ in EC/EMC (3:7, vol%) electrolyte, resulting in the main components of SEI changing from lithium ethylene dicarbonate (LEDC), Li_2CO_3 and LiF to primarily poly (VC). The author suggested that the increased polymeric species in SEI can improve the plating/stripping performance of lithium metal in carbonate electrolytes, thus significantly improving the electrochemical performance of Cu|LFP AFLMBs (Fig. 7B) [159]. However, the performance improvements are accompanied by an increased voltage hysteresis owing to the high resistance of polymeric species in SEI. Thus, an SEI with an optimal balance of organic and inorganic components is still needed to keep exploring.

Solid-state electrolyte

Similar to traditional liquid LMBs, one of the obstacles to the development of AFLMBs is the growth of Li dendrites/whiskers during the Li plating process, which would result in Li loss due to low reversibility and internal short circuits in the battery and further trigger a series of safety issues such as fire hazards and even explosions [160–162]. This has led to widespread interest in developing and using solid-state electrolytes (SSEs) for LMBs and AFLMBs, for their several advantages such as non-flammable properties, high mechanical strength and modulus, as well as relatively good interfacial compatibility toward Li metal [65, 163–165].

However, despite these promises, the development of solid-state AFLMB still faces many challenges [166–169]. First, most of the SSEs, such as $Li_7La_3Zr_2O_{12}$ (10^{-4}–10^{-3} S cm^{-1} @ 25–60°C) [170], $Li_{1+x}Al_xTi_{2-x}(PO_4)_3$ (10^{-5}–10^{-3} S cm^{-1} @ 25–60°C) [171], $Li_{3x}La_{2/3-x}TiO_3$ (10^{-5}–10^{-3} S cm^{-1} @ 25–60°C) [172],

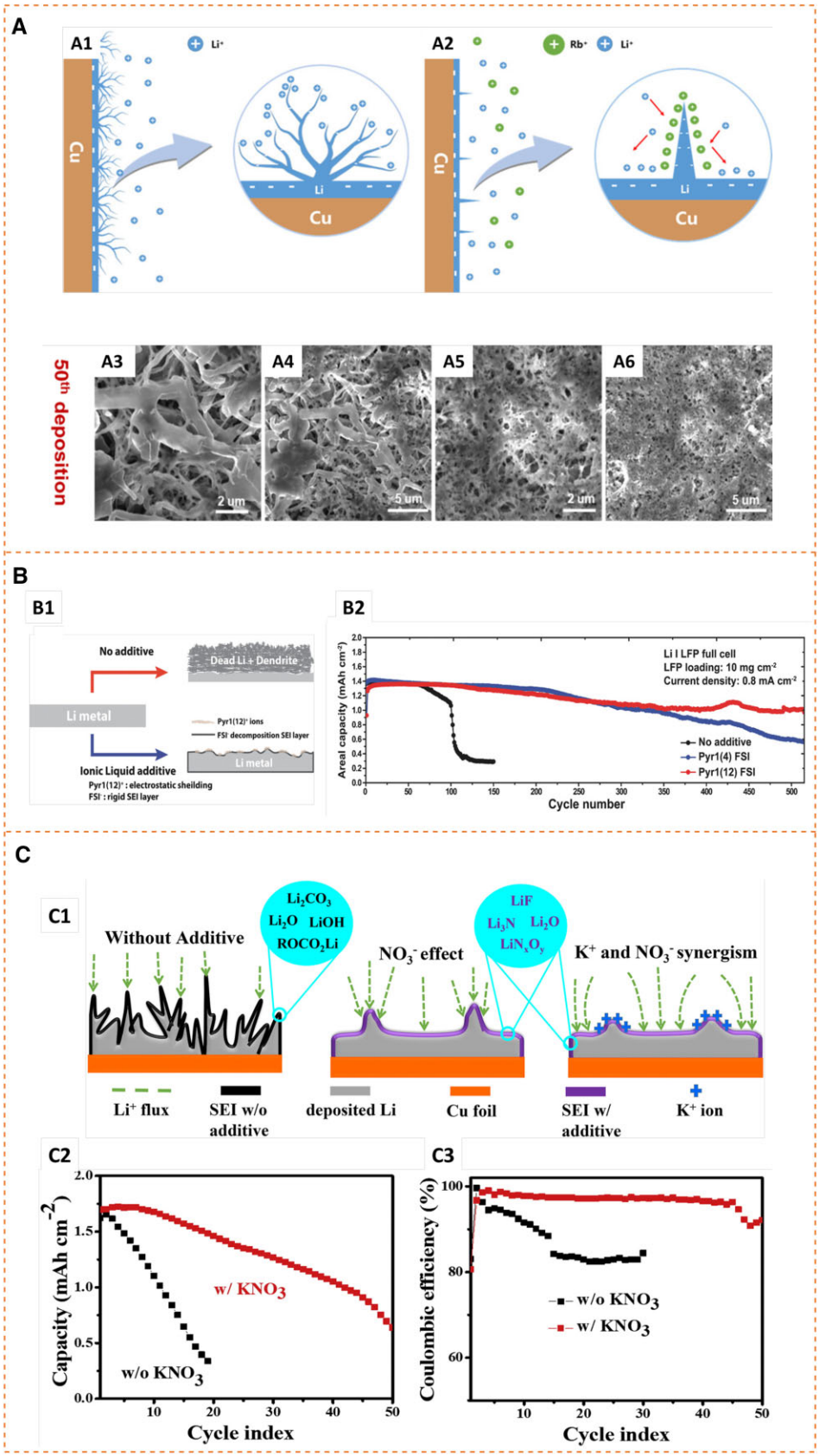

Figure 6: (**A**) Schematic illustration of (**A1**) lithium dendrites growth process and (**A2**) lithium dendrites growth process inhibited by the use of RbF additives. SEM images of the lithium deposition morphology in Cu anode for the 50th deposition (**A3**, **A4**) without RbF and (**A5**, **A6**) with 0.05 M RbF. Reproduced from Ref. [153]. (**B**) **B1**, Schematic representation shows the effect of ionic liquid additive on the stability of Li metal interface and **B2**, the capacity retentions of the Li||LFP coin cells in different electrolytes cycled at a current density of 0.8 mA cm^{-2}. Reproduced from Ref. [154]. (**C**) **C1**, Schematic illustration of lithium decomposition in different electrolytes. The (**C2**) discharge capacities and (**C3**) coulombic efficiencies of Cu||NMC anode-free coin cells with (w/) and without (w/o) KNO_3, cycled at 0.2mAcm^{-2}. Reproduced from Ref. [155].

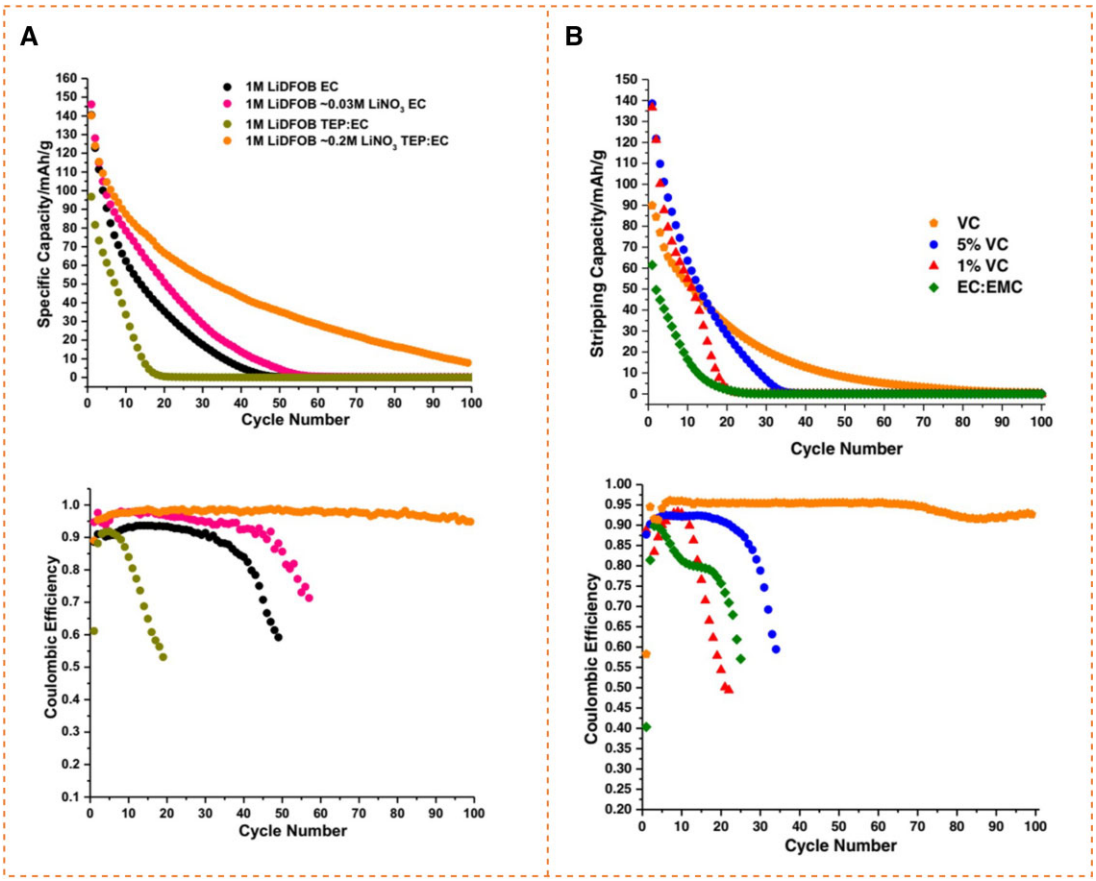

Figure 7: Stripping capacity (above) and CE (below) versus cycle number for (**A**) a series of electrolytes and (**B**) 1.2-M $LiPF_6$ salt in EC:EMC (1:1, v:v), EC:EMC with 1% wt. VC, EC:EMC with 5% wt. VC and VC solvent (VC-S) electrolytes for LFP||Cu anode-free cells at a current density of 0.1 mA cm^{-2}. Reproduced from Refs. [158, 159].

$Li_{1+x}Al_xGe_{2-x}(PO_4)_3$ (10^{-4}–10^{-3} S cm^{-1} @ 25–60°C) [173], $Li_xPO_yN_z$ (LiPON, $x = 2y + 3z - 5$, 10^{-8}–10^{-6} S cm^{-1} @ 25–60°C) [174], polyethylene oxide (10^{-7} - 10^{-3} S cm^{-1} @ 25 - 60°C) [175, 176], etc., have relatively low ionic conductivity at room temperature. Even with additional optimization (e.g. elemental doping [177, 178], ionic substitutions [179], tuning synthesis conditions [180, 181], etc.), it is still difficult to achieve the current ionic conductivity levels of liquid electrolytes. Therefore, these SSEs require high-temperature operation (above 60°C) to attain suitable electrochemical performance, with however high-temperature conditions hindering their practical application prospects. Sulfide-based SSEs possess higher ionic conductivities, comparable to liquid electrolytes, with thus more practical prospects. However, their high reactivity requires handling and cell assembly to be carried out in an inert atmosphere (Argon, nitrogen, dry-air) since these are known to react rapidly with moisture to decompose and form toxic H_2S gas. Their electrochemical stability window is also narrower and in contact with Li metal sulfide SSEs are prone to reduction and generation of ionically blocking films, which will increase the cell impedance.

Another considerable disadvantage of SSEs is the high interfacial resistance due to the poor mechanical contact between SSEs and electrode materials. Moreover, with the volume expansion and contraction of the electrode materials during cycling, the interfacial contact may be gradually lost. Finally, the manufacturing process of the SSEs remains thus far complicated, resulting in high costs. For example, oxide-based SSE requires high-temperature sintering to reduce the grain boundary resistance. Therefore, despite the great promises of this technology, there is still a long way to go to realize the practical applications of solid-state LMBs and AFLMB.

Nevertheless, the realization of SSE-based LMBs and AFLMBs has been attempted already decades ago, particularly driven by the need to develop solid-state micro-batteries. For example, as mentioned in the 'Introduction' part, in 2000, Neudecker *et al.* [74] used LiPON-SSE. They designed a Li-free thin-film battery, with the LCO |LiPON|Cu|Overlayer configuration (Fig. 8A), by using a radio frequency magnetron sputtering thin-film deposition technique [74]. The overlayer consists of either 0.3–1 μm of LiPON-SSE or 6 μm of parylene C and it was deposited onto the Cu anode CC. The authors found that the cell without an overlayer exhibits fast capacity decay due to the generation of blossom-like features on the Cu surface. They believe that the plated Li on the Cu anode CC during the charging process will diffuse through the grain boundaries in the Cu anode CC and reaction with the residual O_2 and H_2O in the Ar-filled bottle to form Li_2O and LiOH, respectively. This is plausible because our previous study has revealed that Li can diffuse into Cu CC through three types of diffusion: (i) A-Type, Li directly diffuses from the surface into Cu through the lattice (bulk); (ii) B-Type, Li first diffuses along grain boundaries and subsequently diffuses from these defects into the bulk and (iii) C-Type, Li predominately diffuses along grain boundaries. Moreover, the diffusion through grain boundary is much faster than through lattice [182]. A gastight overlayer deposited onto the Cu anode CC would eliminate exposure of the plated Li underneath the

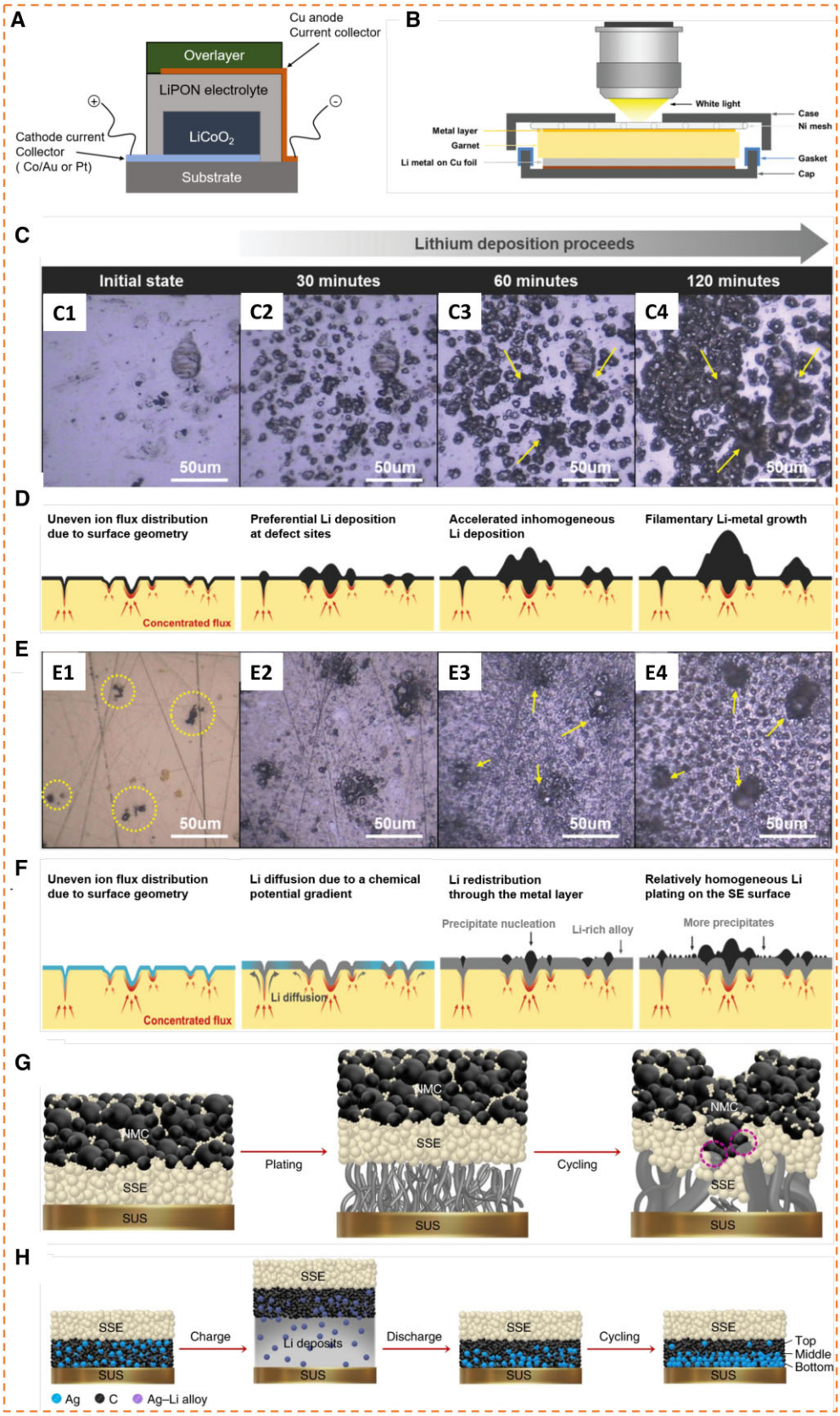

Figure 8: Schematic cross-sectional views of (**A**) a Li-free thin-film battery [74] and (**B**) a coin-type anode-free half-cell. Reproduced from Ref. [183]. (**C, E**) *In operando* optical microscopy images and (**D, F**) schematic diagram showing the uneven Li-ion flux triggered by surface geometry and the corresponding inhomogeneous Li plating (C, D), and Li redistribution through the Au layer and Li nucleation (E, F). Reproduced from Ref. [183]. Schematic of Li plating–stripping on the CC (**G**) without and (**H**) with Ag–C nanocomposite layer during charging and discharging processes. Reproduced from Ref. [68].

anode CC to residual O_2 and H_2O and thereby avoid the thermodynamic potential for the plated Li to diffuse to the surface of the Cu anode CC. So, they also called this overlayer 'Li diffusion blocking overlayer'. The cell achieved excellent capacity retention of 80% after 1000 cycles at a current density of 1.0 mA cm^{-2}, which is an important progress in combining SSEs with AFLMBs configuration. However, targeting the micro-battery application, the cell was designed with a low areal capacity of 100 μAh cm^{-2}, implying high costs and batch manufacture, thus not compatible with large-scale applications as required for electric vehicles and portable devices. However, this work provided valuable insight into the future design of similar systems. For instance, by investigating the surface morphology of the Cu anode CC after cycling, the authors found that the overlayer is essential for enabling cycling stability as it can suppress the formation of Li dendrites. Without the overlayer, the cells exhibited fast capacity decay due to the generation of a large amount of Li dendrites.

Kim *et al.* [183] explored the Li deposition behavior at the interface of an LLZO-based solid-state AFLMB by also directly visualizing the Li deposition morphology using in-operando optical microscopy (Fig. 8B). As shown in Fig. 8C and schematized in Fig. 8D, the Li deposition was found to be affected by the surface morphology of LLZO, in contact with the Ni CC, with the surface defects acting as the preferred sites for Li nucleation. The authors noted that the morphological defect sites (e.g. small scratches, holes and cracks) could trigger localized high electric fields with concentrated Li-ion flux at these locations, resulting in Li metal deposition as islands rather than as uniform thin films, with further grow and fuse to form filamentary Li. In contrast, an LLZO SSE modified with an artificial lithophilic interlayer (e.g. Au and Ag) induced a uniform electric field and Li-ion flux. For example, LLZO coated with a thin (∼5 nm) Au layer will first form a Li–Au alloy (Fig. 8E and F), which was suggested to enable rapid diffusion of Li ions out of defective sites, resulting in relatively uniform Li deposition. In addition, the authors also explored the effect of different interlayer materials, such as Au, Ag and Si, on the Li deposition/dissolution behavior. It is shown that the Ag interlayer has the lowest Li nucleation barriers and the fastest Li deposition/dissolution kinetics and induces a much more uniform and homogenous Li deposition/dissolution reactions among the three interlayer materials. The better efficacy of the Li deposition/dissolution behavior with the Ag interlayer was further confirmed by the electrochemical testing of solid-state AFLMBs including half-cell configuration (CC|interlayer|LLZO|Li) and full cell configuration (CC|interlayer|LLZO|NMC111). The cells with Ag interlayer exhibited much better CEs in both cases. The excellent Li deposition/dissolution behavior endowed by the Ag interlayer might be attributed to its high solubility of Li, which can offer low interfacial energy between Li and Ag by forming a chemically compatible interface during the nucleation process of Li metal, thus influencing the Li deposition behavior and kinetics favorably [183]. This study broadens the understanding of the electrochemical Li deposition/dissolution behavior in solid-state AFLMBs and highlights the importance of exploring suitable interlayer materials as an alternative strategy for regulating Li deposition/dissolution process in solid-state AFLMBs.

Relying on this rationale, Lee *et al.* [68] reported a high-performance solid-state AFLMBs, with the overall structure of NMC|SSE|Ag–C|Cu, by using Li_6PS_5Cl (LPSCl, 10^{-3}–10^{-2} S cm^{-1} @ 25–60°C) as SSE and $LiNi_{0.90}Co_{0.05}Mn_{0.05}O_2$ (NMC) as cathode material. To maintain the interfacial stability between the high-voltage NMC and LPSCl, the surface of the NMC particles was coated with a thin layer of Li_2O–ZrO_2 by the sol–gel method. On the anode side, a nanocomposite layer of Ag nanoparticles (∼23 wt.%) and carbon black with a total thickness of 5 μm was used between the SSE and the stainless-steel CC serving as a buffer layer, but also presumably as lithium-ion storage material. According to the authors, the carbon black acts as a physical separator (despite remaining an electron conductor) to prevent the SSE from direct contact with Li metal thus preventing the decomposition of LPSCl SSE (Fig. 8G and H). The Ag nanoparticles were suggested to serve as nucleation seeds for Li deposition by forming an Ag–Li alloy first in the Ag–C nanocomposite layer and then part of the Ag moves to the CC and forms a solid solution with Li metal, thereby realize uniform, dense and dendrite-free Li plating on the CC surface (Fig. 8H). The respective AFLMB was shown with excellent electrochemical performance in a 0.6-Ah class pouch cell format. Specifically, after 600 and 1000 cycles at a current density of 0.5 C (i.e. 3.4 mA cm^{-2}) with a cathode capacity loading of 6.8 mAh cm^{-2}, the cell retained 95% and 89% of the initial capacity, respectively, with an average CE greater than 99.8%. However, these excellent cell performances were attained under the combined conditions of high temperature (60°C) and extra external pressure (a uniaxial stack pressure of 2–4 MPa) during the cell operation. The operating temperature plays a critical role in the Li-ion conductivity of SSE and interfacial resistances of solid-state LMB. As the temperature decreased, the resistance of solid-state LMB increased and the Li-ion conductivity of SSE decreased and the capacity decreased accordingly. The discharge capacity at 25°C decreased to 90.7% which is lower than that attained at 60°C (99.5%) under a current density of 0.1 C. On the other hand, extra external pressurization is essential for a uniform interface formation and stable Li deposition in solid-state LMB. It can improve the solid–solid interface characteristics and the contact loss problems during cycling. Without external pressure, the cell shows a slightly lower discharge capacity at a low current density (0.1 C). The technical drawbacks are that a temperature of 60°C and an additional external pressure were required for the cell operation to attain a good cycling performance.

The current technological status of solid-state AFLMB is still in the early development stage, with only a few relevant reports thus far. Further efforts should be devoted to the following aspects:

1. Interfacial contact issue between SSEs and anode CC: Generally, the surface of bare CC is tougher than that of Li metal, so the anode/SSE contact interface in solid-state AFLMB is commonly much worse compared with solid-state LMB, resulting in a high interfacial resistance, which will greatly decrease the kinetics of the electrochemical reactions. Currently, the main solution to improve interfacial contact between SSE and anode CC to reduce the interfacial resistance is to apply external pressure during cell operation. On the other hand, increasing the cell operation temperature can also reduce the interface resistance to some extent. However, the external pressure and high operation temperature will also become the key technical drawbacks in practical applications. Therefore, future research should focus on finding a much more suitable technical solution that can maintain good interfacial contact to get rid of the constraints of working conditions such as additional external pressure and high temperature. For example, designing a suitable solid-state AFLMB testing device that can provide sufficient internal pressure to maintain good SSE/CC interfacial contact without extra external pressure. Besides, the

introduction or *in situ* fabrication of a soft artificial interphase layer between the CC and the SSE is also an effective strategy to decrease the interfacial resistance due to conformal contact [184, 185].

2. Li nucleation and growth behavior at SSE/anode CC interface: The Li deposition behavior on the anode CC will affect the CE and thus the performance of solid-state AFLMB [183]. The formation of Li dendrites/whiskers during the Li plating process will lead to Li loss due to low reversibility (e.g. easy to convert into dead Li during cycling) [186, 187]. Therefore, reversible and uniform Li plating/stripping on anode CC is required for solid-state AFLMB to attain good performance. Unlike liquid electrolytes, the Li nucleation/growth in solid-state AFLMB is affected by the type of CC and the surface defects of SSE [183]. In terms of anode CC, the most widely used Cu CC commonly exhibits a high Li nucleation barrier which results in large overpotential accordingly. The Li nucleation barrier will be significantly lower when using CC materials with a higher solubility of Li, such as Au, Ag, Mg, Zn, etc. [68, 183, 188]. For the SSE, as mentioned above, the morphological defect sites (e.g. small scratches, holes and cracks) will lead to the formation of filamentary Li [183]. Thus, future studies should also focus on designing/modifying the anode CC or SSE interface to achieve a highly reversible, stable and dendrite-free Li plating/stripping process. For example, designing new CC material with high Li solubility or modifying Cu CC with a lithophilic coating layer, as well as developing effective strategies (e.g. polishing and coating) to reduce the SSE surface defects.
3. Interfacial stability between SSE and plated Li: Li-ions will sink during the anodic reaction to form a stable SEI and are unavailable for further battery cycling. This should be avoided in solid-state AFLMBs as it directly reduces the Li inventory. Therefore, a stable or chemically inert SSE/plated Li interface is theoretically required for a solid-state AFLMB. However, most of the SSEs are thermodynamically unstable against Li metal. This means that the plated Li might first be used to form the SEI until the stable SSE/plated Li interface is formed, resulting in Li loss in the subsequent cycles. Thus, future research should develop more strategies to improve this issue. Such as designing new SSEs that are intrinsically stable against Li metal and performing an artificial SEI or a protective coating that is stable against Li metal on SSE/anode CC surface.
4. Transfer/calibrate laboratory-level solid-state AFLMB knowledge/techniques/strategies to practical application-level solid-state AFLMB systems: For the anode side, many strategies for improving solid-state AFLMB have been successfully confirmed at the laboratory level. However, in most cases, directly transferring these strategies to practical cell systems is a great challenge and some are not very suitable. For example, although the lithiophilic coating or protective layer on the anode CC/SSE surface can improve the cycle stability of laboratory-level solid-state AFLMBs, its application in practical cell systems may greatly reduce the energy density and weaken the actual advantages of solid-state AFLMBs. Therefore, future studies should also pay more attention to rational application techniques to realize these solutions in practical battery systems.

OUTLOOK AND PERSPECTIVES

AFLMB design sets very challenging targets, with aspects such as high energy metrics, low costs and simple manufacture being mostly advanced. However, the dismissal of graphite anode (for a Li-ion) or Li-metal film (for LMBs) brings further advantages of, for instance, better raw (and potentially critical raw) material economy. Pushing further this rationale and also driven by so much controverted Cobalt sourcing, Nickel price soaring, one can also consider replacing the conventional inorganic cathode materials with more sustainable alternatives. Organic electrode materials emerge as one of the most promising candidates for future energy storage devices, given their generally green and sustainable raw materials supply, low environmental footprint, high chemical diversity as well as competitive energy and power performances [189–198]. Depending on the electrochemical redox center functionality reported in the literature thus far, there are 10 classes of organic electrode materials [192, 199]. Further, these can be divided into p-type materials (anions used for charge compensation) and n-type materials (cations used for charge compensation) [200].

However, despite the richness of organic electrode chemistries, with nearly a thousand compounds tested and reported thus far, no organic positive electrode materials have been applied thus far to build AFLMB. The main reason behind this stalled progress is, in fact, the lack of suitable positive electrode materials. For an anode-free cell design to be operational, a Li-containing or Li-reservoir n-type cathode must be used, like for conventional Li-ion inorganic cathode materials (Fig. 9A). Another alternative is the use of p-type organic cathode (Fig. 9B) materials, resulting in dual-ion cells, with the cathode material upon assembly required to be in the reduced state. It has to be also noted that the n-type organic cathode materials in the oxidized state (Li-host, alike the most used so far organic battery materials) are suitable only for LMB assembly.

The dual-ion mechanism of p-type organic cathodes is in principle feasible but requires an excess amount of electrolyte to compensate for the electrolyte depletion during cell operation. The electrolyte concentration variation as well as other often neglected parameters (e.g. the amount of electrolyte, cell architecture and electrode preparation during charge/discharge) may also affect the plating/stripping efficiency [203]. Another practical drawback of the dual-ion cell based on an organic p-type cathode is that the mass of counter anions should be also considered for specific capacity calculations, which will lower the energy density of the battery cell.

Thus, the most suitable organic cathode candidates for the AFLMB design remain the n-type Li-reservoir materials (Fig. 9A) [192, 204–206]. Despite the early stages of research on these types of materials, there are two emerging classes of organic n-type Li-reservoir compounds reported thus far: conjugated phenolates [204–206] and conjugated sulfonamides [192]. From the energy density point of view, these can reach a specific capacity of 100–230 mAh g^{-1} and operate at a redox potential of 2.4–3.5 V versus Li^+/Li, with thus energy density ranging from 250 to 500 Wh kg^{-1} [192, 204–209].

Finally, one must consider the fundamental and practical difficulties of the organic cathode-based AFLMBs. Organic cathodes generally have low redox potential and high material solubility, which could lead to lower energy density and CE resulting in short battery life compared with inorganic cathodes. If organic AFLMBs are to emerge in the future commercial market, these problems should be addressed properly. By proposing an anode-free organic battery, we hope 1 day in the future, the portable batteries will be constructed in a much greener route without having much complex processing.

Apart from the hitherto advances that happened in AFLMBs, many challenges have to be addressed to meet the benchmark requirements to ensure their commercialization. One of the

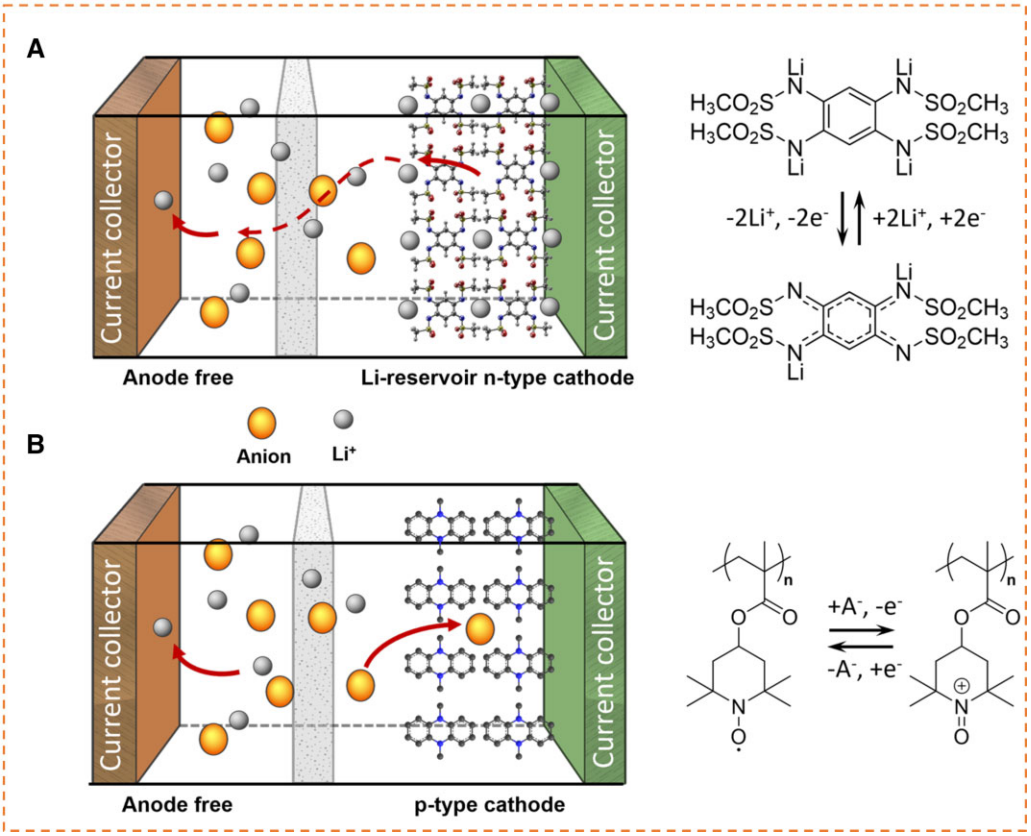

Figure 9: Schematic drawing of the working principle of organic positive electrode materials with potential applicability for AFLMC. Two classes of organic electrode materials are compatible with this cell design technology: (**A**) Li-reservoir n-type materials, like conventional inorganic Li-ion cathodes [201] and (**B**) p-type materials, resulting in the fabrication of dual-ion cells [202].

primary concerns resides in the accomplishment of a high average CE of >99.98%, to withstand the cell above 1000 cycles with >80% of the initial capacity retention. A profound electrochemical–mechanical understanding of the lithium metal coupling with different battery conditions is highly desirable to develop various fabrication and testing protocols, including stacking pressure, initial formation step, charge/discharge cycles, etc., that can efficiently mitigate the various undesirable Li-inventory losses, such as 'dead Li' formation and inhomogeneous creation of mossy Li, etc., which leads to cell failure. Further, optimization of different electrolyte formulations that can induce a smooth, compact, inorganic-rich SEI layer, which can effectively inhibit the lithium dendrite formations, is highly required to improve the CE and long-term cycling stability of AFLMBs. An integration of dual-salt electrolytes, with the concept of LHCEs, which inherit the excellent lithium stabilization property of HCEs with low viscosity and high wettability of conventional electrolytes, might be a promising strategy to stabilize the lithium striping and plating process that can enhance the cell performances. Additionally, tuning the SEI layer compositions and properties via modifications in the solvent structure with fluorinated compounds or via the addition of electrolyte additives such as FEC, VC, etc., can be considered. Further, to ensure the scalability of AFLMBs, more emphasis should be given to developing these innovative strategies in such a way that they can be fitted with the practical cell parameters such as large-area pouch cell and lean electrolyte conditions. Developing SSE formulations attains special attention toward the development of highly safe, non-leaky solid-state AFLMBs.

In solid-state AFLMBs, many efforts should be devoted to tackling various issues related to the large interfacial resistances between the SSEs and anode CC, instability of SSE with the plated Li and surface defects at the SSE as well as the anode CC. In addition to the application of high external pressure and high temperature, different approaches such as fabrication of soft artificial interphase layer or protective coating between the anode CC and SSE to decrease interfacial resistances, modification of anode CC with 'lithiophilic' materials to increase reversibility with high CE and polishing SSE electrolyte surface to reduce defects, are greatly appealing toward the advancement of solid-state AFLMBs. However, the direct transfer of these technologies from the laboratory level to the practical application level remains highly challenging, which requires strenuous effort toward developing novel rational application techniques to realize the solid-state AFLMBs convenient to the practical battery levels. Furthermore, selecting suitable cathode material is also essential and requires advanced investigations, especially while switching from inorganic to organic material, which is greener in the path of developing sustainable and environmentally friendly next-generation anode-free batteries. Finally, it is quite inevitable to amalgamate various interdisciplinary research areas, for instance, customizing *in situ* microscopic and spectroscopic techniques in synchronization with the electrochemical charging/discharging provides real-time insights into the Li electrodeposition/dissolution and SEI layer formations, which could be corroborated by developing new theoretical models, which would unlock novel directions to realize substantial advances in both liquid and solid-state AFLMBs. We hope this

review will open new prospects in the area of anode-free batteries.

ACKNOWLEDGEMENTS

X.Z. acknowledges CSC Scholarships for financial support. A.V. acknowledges CF-ARC grant (18/23-093) MICROBAT for financial support.

AUTHORS' CONTRIBUTIONS

S.P. and A.V. have decided the review topic, directions and title. S.P. has written abstract, introduction partly with X.Z., optimizations of test protocols, out-look and perspective partially with J.W. X.Z., X.L. and J.W. have contributed for the chapters—modifications of electrolyte, SSE, out-look and perspective, respectively. B.B. and A.V. have reviewed the manuscript including figures and provided major scientific corrections.

CONFLICT OF INTEREST STATEMENT

The authors declare no conflict of interest.

References

1. Zachman MJ, Tu Z, Choudhury S *et al.* Cryo-STEM mapping of solid–liquid interfaces and dendrites in lithium-metal batteries. *Nature* 2018;**560**:345–9.
2. Weber R, Genovese M, Louli A *et al.* Long cycle life and dendrite-free lithium morphology in anode-free lithium pouch cells enabled by a dual-salt liquid electrolyte. *Nat Energy* 2019;**4**:683–9.
3. Cheng X-B, Zhang R, Zhao C-Z *et al.* Toward safe lithium metal anode in rechargeable batteries: a review. *Chem Rev* 2017;**117**:10403–73.
4. Zhang J-G. Anode-less. *Nat Energy* 2019;**4**:637–8.
5. Liu Z, Huang Y, Huang Y *et al.* Voltage issue of aqueous rechargeable metal-ion batteries. *Chem Soc Rev* 2020;**49**: 180–232.
6. Zhang Q, Luan J, Tang Y *et al.* Interfacial design of dendrite-free zinc anodes for aqueous zinc-ion batteries. *Angew Chem Int Ed* 2020;**59**:13180–91.
7. Liu X, Depaifve S, Leyssens T *et al.* Versatile synthesis of vanadium(III, IV, V) oxides@reduced graphene oxide nanocomposites and evaluation of their lithium and sodium storage performances. *Batter Supercaps* 2019;**2**:1016–25.
8. Ashish AG, Arunkumar P, Babu B *et al.* $TiNb_2O_7$/graphene hybrid material as high performance anode for lithium-ion batteries. *Electrochim Acta* 2015;**176**:285–92.
9. Boz B, Dev T, Salvadori A, *et al.* Review—electrolyte and electrode designs for enhanced ion transport properties to enable high performance lithium batteries. *J Electrochem Soc* 2021;**168**:090501.
10. Babu B, Shaijumon MM. Studies on kinetics and diffusion characteristics of lithium ions in $TiNb_2O_7$. *Electrochim Acta* 2020;**345**:136208.
11. Arunkumar P, Ashish AG, Babu B *et al.* Nb_2O_5/graphene nanocomposites for electrochemical energy storage. *RSC Adv* 2015;**5**:59997–60004.
12. Varghese SP, Babu B, Prasannachandran R *et al.* Enhanced electrochemical properties of Mn_3O_4/graphene nanocomposite as efficient anode material for lithium ion batteries. *J Alloys Compd* 2019;**780**:588–96.
13. Vlad A, Singh N, Galande C *et al.* Design considerations for unconventional electrochemical energy storage architectures. *Adv Energy Mater* 2015;**5**:1402115.
14. Kwak W-J, RosySharon D *et al.* Lithium–oxygen batteries and related systems: potential, status, and future. *Chem Rev* 2020;**120**:6626–6683.
15. Robinson JB, Xi K, Kumar RV *et al.* 2021 roadmap on lithium sulfur batteries. *J Phys Energy* 2021;**3**:031501.
16. Tarascon J-M. Na-ion versus Li-ion batteries: complementarity rather than competitiveness. *Joule* 2020;**4**:1616–1620.
17. Ponrouch A, Bitenc J, Dominko R *et al.* Multivalent rechargeable batteries. *Energy Storage Mater* 2019;**20**:253–62.
18. Kubota K, Dahbi M, Hosaka T *et al.* Towards K-ion and Na-ion batteries as "beyond Li-ion". *Chem Rec* 2018;**18**:459–479.
19. Liu X, Wang J, Du M *et al.* Unlocking the electrochemistry and the activation mechanism in the iron-rich $Na_{0.6}Fe_{1.2}PO_4$ phase for high-performance sodium-ion storage. *Batter Supercaps* 2022;**5**:e202100390.
20. Wang J, Vlad A. Empowering magnesium. *Nat Energy* 2020;**5**: 945–6.
21. Palaniselvam T, Babu B, Moon H *et al.* Tin-containing graphite for sodium-ion batteries and hybrid capacitors. *Batter Supercaps* 2021;**4**:173–82.
22. Sánchez-Díez E, Ventosa E, Guarnieri M *et al.* Redox flow batteries: status and perspective towards sustainable stationary energy storage. *J Power Sources* 2021;**481**:228804.
23. Li Y, Lu J. Metal-air batteries: will they be the future electrochemical energy storage device of choice? *ACS Energy Lett* 2017;**2**:1370–7.
24. Olabi AG, Sayed ET, Wilberforce T *et al.* Metal-air batteries—a review. *Energies* 2021;**14**:7373.
25. Zheng R, Yu H, Zhang X *et al.* A $TiSe_2$-graphite dual ion battery: fast Na-ion insertion and excellent stability. *Angew Chem Int Ed* 2021;**60**:18430–7.
26. Zhang L, Wang H, Zhang X *et al.* A review of emerging dual-ion batteries: fundamentals and recent Advances. *Adv Funct Mater* 2021;**31**:2010958.
27. Vlad A, Singh N, Rolland J *et al.* Hybrid supercapacitor-battery materials for fast electrochemical charge storage. *Sci Rep* 2014;**4**:4315.
28. Bhat SSM, Babu B, Feygenson M *et al.* Nanostructured $Na_2Ti_9O_{19}$ for hybrid sodium-ion capacitors with excellent rate capability. *ACS Appl Mater Interfaces* 2018;**10**:437–47.
29. Babu B, Ullattil SG, Prasannachandran R *et al.* Ti^{3+} induced brown TiO_2 nanotubes for high performance sodium-ion hybrid capacitors. *ACS Sustainable Chem Eng* 2018;**6**:5401–12.
30. Babu B, Lashmi PG, Shaijumon MM. Li-ion capacitor based on activated rice husk derived porous carbon with improved electrochemical performance. *Electrochim Acta* 2016;**211**: 289–96.
31. Varghese SP, Babu B, Surendran V *et al.* γ-MnOOH-graphene nanocomposite as promising anode material for Li-ion capacitors. *J Energy Storage* 2022;**47**:103636.
32. Babu B, Shaijumon MM. High performance sodium-ion hybrid capacitor based on $Na_2Ti_2O_4(OH)_2$ nanostructures. *J Power Sources* 2017;**353**:85–94.
33. Grey CP, Hall DS. Prospects for lithium-ion batteries and beyond—a 2030 vision. *Nat Commun* 2020;**11**:6279.
34. Rahner D, Machill S, Schlörb H *et al.* Intercalation materials for lithium rechargeable batteries. *Solid State Ion* 1996;**86–88**: 891–6.

35. Asenbauer J, Eisenmann T, Kuenzel M *et al.* The success story of graphite as a lithium-ion anode material—fundamentals, remaining challenges, and recent developments including silicon (oxide) composites. *Sustain Energy Fuels* 2020;**4**:5387–416.
36. Choi JW, Aurbach D. Promise and reality of post-lithium-ion batteries with high energy densities. *Nat Rev Mater* 2016;**1**: 16013.
37. Li P, Kim H, Myung S-T *et al.* Diverting exploration of silicon anode into practical way: a review focused on silicon–graphite composite for lithium ion batteries. *Energy Storage Mater* 2021;**35**:550–76.
38. Eshetu GG, Zhang H, Judez X *et al.* Production of high-energy Li-ion batteries comprising silicon-containing anodes and insertion-type cathodes. *Nat Commun* 2021;**12**:5459.
39. Eshetu GG, Figgemeier E. Confronting the challenges of next-generation silicon anode-based lithium-ion batteries: role of designer electrolyte additives and polymeric binders. *ChemSusChem* 2019;**12**:2515–39.
40. Tang S, Qiu Z, Wang X-Y *et al.* A room-temperature sodium metal anode enabled by a sodiophilic layer. *Nano Energy* 2018;**48**:101–6.
41. Jiao S, Zheng J, Li Q *et al.* Behavior of lithium metal anodes under various capacity utilization and high current density in lithium metal batteries. *Joule* 2018;**2**:110–24.
42. Hou LP, Zhang XQ, Li BQ *et al.* Cycling a lithium metal anode at 90°C in a liquid electrolyte. *Angew Chem* 2020;**132**:15221–5.
43. Li G, Liu Z, Huang Q *et al.* Stable metal battery anodes enabled by polyethylenimine sponge hosts by way of electrokinetic effects. *Nat Energy* 2018;**3**:1076–83.
44. Cheng X-B, Yan C, Zhang X-Q *et al.* Electronic and ionic channels in working interfaces of lithium metal anodes. *ACS Energy Lett* 2018;**3**:1564–70.
45. Liu H, Cheng X-B, Huang J-Q *et al.* Controlling dendrite growth in solid-state electrolytes. *ACS Energy Lett* 2020;**5**: 833–43.
46. Tian Y, An Y, Wei C *et al.* Flexible and free-standing Ti_3C_2Tx MXene@ Zn paper for dendrite-free aqueous zinc metal batteries and nonaqueous lithium metal batteries. *ACS Nano* 2019;**13**:11676–85.
47. Xiao Y, Du F, Hu C *et al.* High-performance Li-CO_2 batteries from free-standing, binder-free, bifunctional three-dimensional carbon catalysts. *ACS Energy Lett* 2020;**5**:916–21.
48. Xu W, Wang J, Ding F *et al.* Lithium metal anodes for rechargeable batteries. *Energy Environ Sci* 2014;**7**:513–37.
49. Lin D, Liu Y, Cui Y. Reviving the lithium metal anode for high-energy batteries. *Nat Nanotech* 2017;**12**:194.
50. Li H. Practical evaluation of Li-ion batteries. *Joule* 2019;**3**: 911–4.
51. Varzi A, Thanner K, Scipioni R *et al.* Current status and future perspectives of lithium metal batteries. *J Power Sources* 2020;**480**:228803.
52. Chen S, Niu C, Lee H *et al.* Critical parameters for evaluating coin cells and pouch cells of rechargeable Li-metal batteries. *Joule* 2019;**3**:1094–105.
53. Albertus P, Babinec S, Litzelman S *et al.* Status and challenges in enabling the lithium metal electrode for high-energy and low-cost rechargeable batteries. *Nat Energy* 2018; **3**:16–21.
54. Liu B, Zhang J-G, Xu W. Advancing lithium metal batteries. *Joule* 2018;**2**:833–45.
55. Zheng J, Engelhard MH, Mei D *et al.* Electrolyte additive enabled fast charging and stable cycling lithium metal batteries. *Nat Energy* 2017;**2**:17012.
56. Wang S-H, Yin Y-X, Zuo T-T *et al.* Stable Li metal anodes via regulating lithium plating/stripping in vertically aligned microchannels. *Adv Mater* 2017;**29**:1703729.
57. Aurbach D, Zinigrad E, Cohen Y *et al.* A short review of failure mechanisms of lithium metal and lithiated graphite anodes in liquid electrolyte solutions. *Solid State Ion* 2002;**148**:405–16.
58. Liu J, Bao Z, Cui Y *et al.* Pathways for practical high-energy long-cycling lithium metal batteries. *Nat Energy* 2019;**4**: 180–6.
59. Hobold GM, Lopez J, Guo R *et al.* Moving beyond 99.9% Coulombic efficiency for lithium anodes in liquid electrolytes. *Nat Energy* 2021;**6**:951–60.
60. Adams BD, Zheng J, Ren X *et al.* Accurate determination of Coulombic efficiency for lithium metal anodes and lithium metal batteries. *Adv Energy Mater* 2018;**8**:1702097.
61. Schmuch R, Wagner R, Hörpel G *et al.* Performance and cost of materials for lithium-based rechargeable automotive batteries. *Nat Energy* 2018;**3**:267–78.
62. Wang MJ, Kazyak E, Dasgupta NP *et al.* Transitioning solid-state batteries from lab to market: Linking electro-chemo-mechanics with practical considerations. *Joule* 2021;**5**: 1371–90.
63. Etxebarria A, Koch SL, Bondarchuk O *et al.* Work function evolution in Li anode processing. *Adv Energy Mater* 2020;**10**: 2000520.
64. Meyer HC. Some practical aspects of handling lithium metal. In: *Handling and Uses of the Alkali Metals*. *American Chemical Society*, 1957, 9–15.
65. Nanda S, Gupta A, Manthiram A. Anode-free full cells: a pathway to high-energy density lithium-metal batteries. *Adv Energy Mater* 2021;**11**:2000804.
66. Tian Y, An Y, Wei C *et al.* Recently advances and perspectives of anode-free rechargeable batteries. *Nano Energy* 2020: 105344.
67. Chen J, Li Q, Pollard TP *et al.* Electrolyte design for Li metal-free Li batteries. *Mater Today* 2020;**39**:118–26.
68. Lee Y-G, Fujiki S, Jung C *et al.* High-energy long-cycling all-solid-state lithium metal batteries enabled by silver–carbon composite anodes. *Nat Energy* 2020;**5**:299–308.
69. Louli A, Eldesoky A, Weber R *et al.* Diagnosing and correcting anode-free cell failure via electrolyte and morphological analysis. *Nat Energy* 2020;**5**:693–702.
70. Xie Z, Wu Z, An X *et al.* Anode-free rechargeable lithium metal batteries: progress and prospects. *Energy Storage Mater* 2020;**31**:386–401.
71. Heubner C, Maletti S, Auer H *et al.* From lithium-metal toward anode-free solid-state batteries: current developments, issues, and challenges. *Adv Funct Mater* 2021;**31**: 2106608.
72. Han P, Han X, Yao J *et al.* Flexible graphite film with laser drilling pores as novel integrated anode free of metal current collector for sodium ion battery. *Electrochem Commun* 2015; **61**:84–8.
73. Cohn AP, Muralidharan N, Carter R *et al.* Anode-free sodium battery through in situ plating of sodium metal. *Nano Lett* 2017;**17**:1296–301.
74. Neudecker BJ, Dudney NJ, Bates JB. "Lithium-free" thin-film battery with in-situ plated Li anode. *J Electrochem Soc* 2000; **147**:517.
75. Zhang W-J. Structure and performance of $LiFePO_4$ cathode materials: a review. *J Power Sources* 2011;**196**:2962–70.
76. Assegie AA, Cheng J-H, Kuo L-M *et al.* Polyethylene oxide film coating enhances lithium cycling efficiency of an

anode-free lithium-metal battery. *Nanoscale* 2018;**10**: 6125–38.
77. Babu B, Simon P, Balducci A. Fast charging materials for high power applications. *Adv Energy Mater* 2020;**10**:2001128.
78. Thackeray MM, Amine K. Layered Li–Ni–Mn–Co oxide cathodes. *Nat Energy* 2021;**6**:933.
79. Liu J, Wang J, Ni Y *et al.* Recent breakthroughs and perspectives of high-energy layered oxide cathode materials for lithium ion batteries. *Mater Today* 2021;**43**:132–65.
80. Asenbauer J, Eisenmann T, Kuenzel M *et al.* The success story of graphite as a lithium-ion anode material—fundamentals, remaining challenges, and recent developments including silicon (oxide) composites. *Sustain Energy Fuels* 2020;**4**:5387–416.
81. Klein S, van Wickeren S, Röser S *et al.* Understanding the outstanding high-voltage performance of NCM523‖graphite lithium ion cells after elimination of ethylene carbonate solvent from conventional electrolyte. *Adv Energy Mater* 2021; **11**:2003738.
82. Peled E. The electrochemical behavior of alkali and alkaline earth metals in nonaqueous battery systems—the solid electrolyte interphase model. *J Electrochem Soc* 1979;**126**: 2047–51.
83. Yu Z, Wang H, Kong X *et al.* Molecular design for electrolyte solvents enabling energy-dense and long-cycling lithium metal batteries. *Nat Energy* 2020;**5**:526–33.
84. Yang Y, Davies DM, Yin Y *et al.* High-efficiency lithium-metal anode enabled by liquefied gas electrolytes. *Joule* 2019; **3**:1986–2000.
85. Xie Z, Wu Z, An X *et al.* Anode-free rechargeable lithium metal batteries: progress and prospects. *Energy Storage Mater* 2020;**32**:386–401.
86. Wang Q, Liu B, Shen Y *et al.* Confronting the challenges in lithium anodes for lithium metal batteries. *Adv Sci* 2021;**8**: 2101111.
87. LePage WS, Chen Y, Kazyak E *et al.* Lithium mechanics: roles of strain rate and temperature and implications for lithium metal batteries. *J Electrochem Soc* 2019;**166**:A89–97.
88. Barai P, Higa K, Srinivasan V. Lithium dendrite growth mechanisms in polymer electrolytes and prevention strategies. *Phys Chem Chem Phys* 2017;**19**:20493–505.
89. Wilkinson DP, Blom H, Brandt K *et al.* Effects of physical constraints on Li cyclability. *J Power Sources* 1991;**36**:517–27.
90. Qin L, Wang K, Xu H *et al.* The role of mechanical pressure on dendritic surface toward stable lithium metal anode. *Nano Energy* 2020;**77**:105098.
91. Yin X, Tang W, Jung ID *et al.* Insights into morphological evolution and cycling behaviour of lithium metal anode under mechanical pressure. *Nano Energy* 2018;**50**:659–64.
92. Monroe C, Newman J. The impact of elastic deformation on deposition kinetics at lithium/polymer interfaces. *J Electrochem Soc* 2005;**152**:A396.
93. Fincher CD, Ojeda D, Zhang Y *et al.* Mechanical properties of metallic lithium: from nano to bulk scales. *Acta Mater* 2020; **186**:215–22.
94. Louli AJ, Genovese M, Weber R *et al.* Exploring the impact of mechanical pressure on the performance of anode-free lithium metal cells. *J Electrochem Soc* 2019;**166**:A1291.
95. Xu C, Ahmad Z, Aryanfar A *et al.* Enhanced strength and temperature dependence of mechanical properties of Li at small scales and its implications for Li metal anodes. *Proc Natl Acad Sci USA* 2017;**114**:57–61.
96. Wang Z, Li X, Chen Y *et al.* Creep-enabled 3D solid-state lithium-metal battery. *Chem* 2020;**6**:2878–92.
97. Masias A, Felten N, Garcia-Mendez R *et al.* Elastic, plastic, and creep mechanical properties of lithium metal. *J Mater Sci* 2019;**54**:2585–600.
98. Yan K, Wang J, Zhao S *et al.* Temperature-dependent nucleation and growth of dendrite-free lithium metal anodes. *Angew Chem Int Ed* 2019;**58**:11364–8.
99. Wang J, Huang W, Pei A *et al.* Improving cyclability of Li metal batteries at elevated temperatures and its origin revealed by cryo-electron microscopy. *Nat Energy* 2019;**4**: 664–70.
100. Genovese M, Louli AJ, Weber R *et al.* Hot formation for improved low temperature cycling of anode-free lithium metal batteries. *J Electrochem Soc* 2019;**166**:A3342–7.
101. Besenhard JO, Wagner MW, Winter M *et al.* Inorganic film-forming electrolyte additives improving the cycling behaviour of metallic lithium electrodes and the self-discharge of carbon–lithium electrodes. *J Power Sources* 1993;**44**:413–20.
102. Zhai P, Liu L, Wei Y *et al.* Self-healing nucleation seeds induced long-term dendrite-free lithium metal anode. *Nano Lett* 2021;**21**:7715–23.
103. Fang C, Lu B, Pawar G *et al.* Pressure-tailored lithium deposition and dissolution in lithium metal batteries. *Nat Energy* 2021;**6**:987–94.
104. Louli AJ, Coon M, Genovese M *et al.* Optimizing cycling conditions for anode-free lithium metal cells. *J Electrochem Soc* 2021;**168**:020515.
105. Matios E, Wang H, Wang C *et al.* Enabling safe sodium metal batteries by solid electrolyte interphase engineering: a review. *Ind Eng Chem Res* 2019;**58**:9758–80.
106. Lee B, Paek E, Mitlin D *et al.* Sodium metal anodes: emerging solutions to dendrite growth. *Chem Rev* 2019;**119**:5416–60.
107. Ernould B, Sieuw L, Barozzino-Consiglio G *et al.* Negative redox potential shift in fire-retardant electrolytes and consequences for high-energy hybrid batteries. *ACS Appl Energy Mater* 2019;**2**:7879–85.
108. Quartarone E, Mustarelli P. Review-emerging trends in the design of electrolytes for lithium and post-lithium batteries. *J Electrochem Soc* 2020;**167**:050508.
109. Babu B, Enke M, Prykhodska S *et al.* New diglyme-based gel polymer electrolytes for Na-based energy storage devices. *ChemSusChem* 2021;**14**:4836–45.
110. Woo J-J, Maroni VA, Liu G *et al.* Symmetrical impedance study on inactivation induced degradation of lithium electrodes for batteries beyond lithium-ion. *J Electrochem Soc* 2014;**161**:A827.
111. Hagos TT, Su W-N, Huang C-J *et al.* Developing high-voltage carbonate-ether mixed electrolyte via anode-free cell configuration. *J Power Sources* 2020;**461**:228053.
112. Qian J, Henderson WA, Xu W *et al.* High rate and stable cycling of lithium metal anode. *Nat Commun* 2015;**6**:1–9.
113. Qian J, Adams BD, Zheng J *et al.* Anode-free rechargeable lithium metal batteries. *Adv Funct Mater* 2016;**26**:7094–102.
114. Nilsson V, Kotronia A, Lacey M *et al.* Highly concentrated LiTFSI–EC electrolytes for lithium metal batteries. *ACS Appl Energy Mater* 2019;**3**:200–7.
115. Yu X, Manthiram A. Electrode–electrolyte interfaces in lithium-based batteries. *Energy Environ Sci* 2018;**11**:527–43.
116. Xu K. Nonaqueous liquid electrolytes for lithium-based rechargeable batteries. *Chem Rev* 2004;**104**:4303–418.
117. Cao X, Jia H, Xu W *et al.* Review—localized high-concentration electrolytes for lithium batteries. *J Electrochem Soc* 2021;**168**:010522.
118. Yamada Y, Furukawa K, Sodeyama K *et al.* Unusual stability of acetonitrile-based superconcentrated electrolytes for

fast-charging lithium-ion batteries. *J Am Chem Soc* 2014;**136**:5039–46.
119. Zhang J-G, Xu W, Xiao J *et al.* Lithium metal anodes with nonaqueous electrolytes. *Chem Rev* 2020;**120**:13312–48.
120. Pande V, Viswanathan V. Computational screening of current collectors for enabling anode-free lithium metal batteries. *ACS Energy Lett* 2019;**4**:2952–9.
121. Yamada Y, Wang J, Ko S *et al.* Advances and issues in developing salt-concentrated battery electrolytes. *Nat Energy* 2019;**4**:269–80.
122. Hosaka T, Kubota K, Kojima H *et al.* Highly concentrated electrolyte solutions for 4 V class potassium-ion batteries. *Chem Commun* 2018;**54**:8387–90.
123. Vatamanu J, Borodin O, Smith GD. Molecular dynamics simulation studies of the structure of a mixed carbonate/LiPF6 electrolyte near graphite surface as a function of electrode potential. *J Phys Chem C* 2012;**116**:1114–21.
124. Ling C, Banerjee D, Matsui M. Study of the electrochemical deposition of Mg in the atomic level: why it prefers the non-dendritic morphology. *Electrochim Acta* 2012;**76**:270–4.
125. Hagos TT, Thirumalraj B, Huang C-J *et al.* Locally concentrated $LiPF_6$ in a carbonate-based electrolyte with fluoroethylene carbonate as a diluent for anode-free lithium metal batteries. *ACS Appl Mater Interfaces* 2019;**11**:9955–63.
126. Ren X, Zou L, Cao X *et al.* Enabling high-voltage lithium-metal batteries under practical conditions. *Joule* 2019;**3**:1662–76.
127. Alvarado J, Schroeder MA, Pollard TP *et al.* Bisalt ether electrolytes: a pathway towards lithium metal batteries with Ni-rich cathodes. *Energy Environ Sci* 2019;**12**:780–94.
128. Yu L, Chen S, Lee H *et al.* A localized high-concentration electrolyte with optimized solvents and lithium difluoro (oxalate) borate additive for stable lithium metal batteries. *ACS Energy Lett* 2018;**3**:2059–67.
129. An SJ, Li J, Daniel C *et al.* The state of understanding of the lithium-ion-battery graphite solid electrolyte interphase (SEI) and its relationship to formation cycling. *Carbon* 2016;**105**:52–76.
130. Markevich E, Salitra G, Chesneau F *et al.* Very stable lithium metal stripping–plating at a high rate and high areal capacity in fluoroethylene carbonate-based organic electrolyte solution. *ACS Energy Lett* 2017;**2**:1321–6.
131. Wang J, Yamada Y, Sodeyama K *et al.* Fire-extinguishing organic electrolytes for safe batteries. *Nat Energy* 2018;**3**:22–9.
132. Zeng Z, Murugesan V, Han KS *et al.* Non-flammable electrolytes with high salt-to-solvent ratios for Li-ion and Li-metal batteries. *Nat Energy* 2018;**3**:674–81.
133. Zhai P, Liu L, Gu X *et al.* Interface engineering for lithium metal anodes in liquid electrolyte. *Adv Energy Mater* 2020;**10**:2001257.
134. Takada K, Yamada Y, Yamada A. Optimized nonflammable concentrated electrolytes by introducing a low-dielectric diluent. *ACS Appl Mater Interfaces* 2019;**11**:35770–6.
135. Wang Z, Qi F, Yin L *et al.* An anion-tuned solid electrolyte interphase with fast ion transfer kinetics for stable lithium anodes. *Adv Energy Mater* 2020;**10**:1903843.
136. Shen X, Ji H, Liu J *et al.* Super lithiophilic SEI derived from quinones electrolyte to guide Li uniform deposition. *Energy Storage Mater* 2020;**24**:426–431.
137. Zheng Q, Yamada Y, Shang R *et al.* A cyclic phosphate-based battery electrolyte for high voltage and safe operation. *Nat Energy* 2020;**5**:291–8.
138. Zhang Z, Hu L, Wu H *et al.* Fluorinated electrolytes for 5 V lithium-ion battery chemistry. *Energy Environ Sci* 2013;**6**:1806–10.
139. Xiao L, Zeng Z, Liu X *et al.* Stable Li metal anode with "ion-solvent-coordinated" nonflammable electrolyte for safe Li metal batteries. *ACS Energy Lett* 2019;**4**:483–8.
140. Tan SJ, Yue J, Hu XC *et al.* Nitriding-interface-regulated lithium plating enables flame-retardant electrolytes for high-voltage lithium metal batteries. *Angew Chem* 2019;**131**:7884–9.
141. Bizot C, Blin M-A, Guichard P *et al.* Aluminum current collector for high voltage Li-ion battery. Part I: a benchmark study with statistical analysis. *Electrochem Commun* 2021;**126**:107013.
142. Beyene TT, Bezabh HK, Weret MA *et al.* Concentrated dual-salt electrolyte to stabilize Li metal and increase cycle life of anode free Li-metal batteries. *J Electrochem Soc* 2019;**166**:A1501.
143. Ding F, Xu W, Chen X *et al.* Effects of carbonate solvents and lithium salts on morphology and Coulombic efficiency of lithium electrode. *J Electrochem Soc* 2013;**160**:A1894–A1901.
144. Zhang H, Eshetu GG, Judez X *et al.* Electrolyte additives for lithium metal anodes and rechargeable lithium metal batteries: progress and perspectives. *Angew Chem Int Ed* 2018;**57**:15002–27.
145. Von Aspern N, Röschenthaler GV, Winter M *et al.* Fluorine and lithium: ideal partners for high-performance rechargeable battery electrolytes. *Angew Chem Int Ed* 2019;**58**:15978–6000.
146. Ma Y, Zhou Z, Li C *et al.* Enabling reliable lithium metal batteries by a bifunctional anionic electrolyte additive. *Energy Storage Mater* 2018;**11**:197–204.
147. Omale JO, Van Velthem P, Antohe V-A *et al.* Effects of electrolyte additives and nanowire diameter on the electrochemical performance of lithium-ion battery anodes based on interconnected nickel–tin nanowire networks. *Energy Technol* 2021;**9**:2100062.
148. Jia H, Wang J, Lin F *et al.* TPPi as a flame retardant for rechargeable lithium batteries with sulfur composite cathodes. *Chem Commun* 2014;**50**:7011–3.
149. Zheng X, Wang X, Cai X *et al.* Constructing a protective interface film on layered lithium-rich cathode using an electrolyte additive with special molecule structure. *ACS Appl Mater Interfaces* 2016;**8**:30116–25.
150. Ding F, Xu W, Graff GL *et al.* Dendrite-free lithium deposition via self-healing electrostatic shield mechanism. *J Am Chem Soc* 2013;**135**:4450–6.
151. Ye H, Yin Y-X, Zhang S-F *et al.* Synergism of Al-containing solid electrolyte interphase layer and Al-based colloidal particles for stable lithium anode. *Nano Energy* 2017;**36**:411–7.
152. Chen Y, Freunberger SA, Peng Z *et al.* Charging a Li-O_2 battery using a redox mediator. *Nat Chem* 2013;**5**:489–94.
153. Li S, Fang S, Dou H *et al.* RbF as a dendrite-inhibiting additive in lithium metal batteries. *ACS Appl Mater Interfaces* 2019;**11**:20804–11.
154. Yoo DJ, Kim KJ, Choi JW. The synergistic effect of cation and anion of an ionic liquid additive for lithium metal anodes. *Adv Energy Mater* 2018;**8**:1702744.
155. Sahalie NA, Assegie AA, Su W-N *et al.* Effect of bifunctional additive potassium nitrate on performance of anode free lithium metal battery in carbonate electrolyte. *J Power Sources* 2019;**437**:226912.
156. Alpen Uv, Rabenau A, Talat G. Ionic conductivity in Li_3N single crystals. *Appl Phys Lett* 1977;**30**:621–3.
157. Xu H, Li Y, Zhou A *et al.* Li_3N-modified garnet electrolyte for all-solid-state lithium metal batteries operated at 40 C. *Nano Lett* 2018;**18**:7414–8.

158. Brown ZL, Heiskanen S, Lucht BL. Using triethyl phosphate to increase the solubility of $LiNO_3$ in carbonate electrolytes for improving the performance of the lithium metal anode. *J Electrochem Soc* 2019;**166**:A2523.
159. Brown ZL, Jurng S, Lucht BL. Investigation of the lithium solid electrolyte interphase in vinylene carbonate electrolytes using Cu‖$LiFePO_4$ cells. *J Electrochem Soc* 2017;**164**:A2186.
160. Zhou Q, Dong S, Lv Z *et al.* A temperature-responsive electrolyte endowing superior safety characteristic of lithium metal batteries. *Adv Energy Mater* 2020;**10**:1903441.
161. Tan S-J, Yue J, Hu X-C *et al.* Nitriding-interface-regulated lithium plating enables flame-retardant electrolytes for high-voltage lithium metal batteries. *Angew Chem Int Ed* 2019;**58**:7802–7807.
162. Zhang Q-K, Zhang X-Q, Yuan H *et al.* Thermally stable and nonflammable electrolytes for lithium metal batteries: progress and perspectives. *Small Sci* 2021;**1**:2100058.
163. Schnell J, Günther T, Knoche T *et al.* All-solid-state lithium-ion and lithium metal batteries—paving the way to large-scale production. *J Power Sources* 2018;**382**:160–75.
164. Wang MJ, Carmona E, Gupta A *et al.* Enabling "lithium-free" manufacturing of pure lithium metal solid-state batteries through in situ plating. *Nat Commun* 2020;**11**:5201.
165. Tong Z, Bazri B, Hu S-F, *et al.* Interfacial chemistry in anode-free batteries: challenges and strategies. *J Mater Chem A* 2021;**9**:7396–406.
166. Fan L, Wei S, Li S *et al.* Recent progress of the solid-state electrolytes for high-energy metal-based batteries. *Adv Energy Mater* 2018;**8**:1702657.
167. Zhou D, Shanmukaraj D, Tkacheva A *et al.* Polymer electrolytes for lithium-based batteries: advances and prospects. *Chem* 2019;**5**:2326–52.
168. Huo H, Chen Y, Luo J *et al.* Rational design of hierarchical "ceramic-in-polymer" and "polymer-in-ceramic" electrolytes for dendrite-free solid-state batteries. *Adv Energy Mater* 2019;**9**:1804004.
169. Zhao C, Liu L, Qi X *et al.* Solid-state sodium batteries. *Adv Energy Mater* 2018;**8**:1703012.
170. Murugan R, Thangadurai V, Weppner W. Fast lithium ion conduction in garnet-type $Li_7La_3Zr_2O_{12}$. *Angew Chem Int Ed* 2007;**46**:7778–81.
171. Morimoto H, Awano H, Terashima J *et al.* Preparation of lithium ion conducting solid electrolyte of NASICON-type $Li_{1+}xAlxTi_{2-}x(PO_4)_3$ ($x = 0.3$) obtained by using the mechanochemical method and its application as surface modification materials of $LiCoO_2$ cathode for lithium cell. *J Power Sources* 2013;**240**:636–43.
172. Inaguma Y, Liquan C, Itoh M *et al.* High ionic conductivity in lithium lanthanum titanate. *Solid State Commun* 1993;**86**:689–93.
173. Fu J. Fast Li^+-ion conducting glass-ceramics in the system Li_2O–Al_2O_3–GeO_2–P_2O_5. *Solid State Ion* 1997;**104**:191–4.
174. Kim YG, Wadley HNG. Lithium phosphorous oxynitride films synthesized by a plasma-assisted directed vapor deposition approach. *J Vac Sci Technol* 2008;**26**:174–83.
175. Pożyczka K, Marzantowicz M, Dygas JR *et al.* Ionic conductivity and lithium transference number of poly(ethylene oxide):LiTFSI system. *Electrochim Acta* 2017;**227**:127–35.
176. Prasanth R, Shubha N, Hng HH *et al.* Effect of poly(ethylene oxide) on ionic conductivity and electrochemical properties of poly(vinylidenefluoride) based polymer gel electrolytes prepared by electrospinning for lithium ion batteries. *J Power Sources* 2014;**245**:283–91.
177. Meesala Y, Liao Y-K, Jena A *et al.* An efficient multi-doping strategy to enhance Li-ion conductivity in the garnet-type solid electrolyte $Li_7La_3Zr_2O_{12}$. *J Mater Chem A* 2019;**7**:8589–601.
178. Le HTT, Kalubarme RS, Ngo DT *et al.* Citrate gel synthesis of aluminum-doped lithium lanthanum titanate solid electrolyte for application in organic-type lithium–oxygen batteries. *J Power Sources* 2015;**274**:1188–99.
179. Thangadurai V, Weppner W. $Li_6ALa_2Ta_2O_{12}$ (A = Sr, Ba): novel garnet-like oxides for fast lithium ion conduction. *Adv Funct Mater* 2005;**15**:107–12.
180. Li G, Li M, Dong L *et al.* Low energy ion beam assisted deposition of controllable solid state electrolyte LiPON with increased mechanical properties and ionic conductivity. *Int J Hydrog Energy* 2014;**39**:17466–72.
181. Suzuki N, Inaba T, Shiga T. Electrochemical properties of LiPON films made from a mixed powder target of Li_3PO_4 and Li_2O. *Thin Solid Films* 2012;**520**:1821–5.
182. Rupp R, Caerts B, Vantomme A *et al.* Lithium diffusion in copper. *J Phys Chem Lett* 2019;**10**:5206–10.
183. Kim S, Jung C, Kim H *et al.* The role of interlayer chemistry in Li-metal growth through a garnet-type solid electrolyte. *Adv Energy Mater* 2020;**10**:1903993.
184. Zhou W, Wang S, Li Y *et al.* Plating a dendrite-free lithium anode with a polymer/ceramic/polymer sandwich electrolyte. *J Am Chem Soc* 2016;**138**:9385–8.
185. Fu K, Gong Y, Liu B *et al.* Toward garnet electrolyte-based Li metal batteries: an ultrathin, highly effective, artificial solid-state electrolyte/metallic Li interface. *Sci Adv* 2017;**3**:e1601659.
186. Li Z, Huang J, Yann Liaw B *et al.* A review of lithium deposition in lithium-ion and lithium metal secondary batteries. *J Power Sources* 2014;**254**:168–82.
187. Steiger J, Richter G, Wenk M *et al.* Comparison of the growth of lithium filaments and dendrites under different conditions. *Electrochem Commun* 2015;**50**:11–4.
188. Yan K, Lu Z, Lee H-W *et al.* Selective deposition and stable encapsulation of lithium through heterogeneous seeded growth. *Nat Energy* 2016;**1**:16010.
189. Poizot P, Gaubicher J, Renault S *et al.* Opportunities and Challenges for organic electrodes in electrochemical energy storage. *Chem Rev* 2020;**120**:6490–6557.
190. Lu Y, Chen J. Prospects of organic electrode materials for practical lithium batteries. *Nat Rev Chem* 2020;**4**:127–42.
191. Lakraychi AE, Dolhem F, Vlad A *et al.* Organic negative electrode materials for metal-ion and molecular-ion batteries: progress and challenges from a molecular engineering perspective. *Adv Energy Mater* 2021;**11**:2101562.
192. Wang J, Lakraychi AE, Liu X *et al.* Conjugated sulfonamides as a class of organic lithium-ion positive electrodes. *Nat Mater* 2021;**20**:665–73.
193. Esser B, Dolhem F, Becuwe M *et al.* A perspective on organic electrode materials and technologies for next generation batteries. *J Power Sources* 2021;**482**:228814.
194. Lakraychi AE, De Kreijger S, Gupta D *et al.* Phendione-transition-metal complexes with bipolar redox activity for lithium batteries. *ChemSusChem* 2020;**13**:2225–31.
195. Sieuw L, Jouhara A, Quarez E *et al.* A H-bond stabilized quinone electrode material for Li-organic batteries: the strength of weak bonds. *Chem Sci* 2019;**10**:418–26.
196. Cheng L, Du X, Jiang Y *et al.* Mechanochemical assembly of 3D mesoporous conducting-polymer aerogels for high performance hybrid electrochemical energy storage. *Nano Energy* 2017;**41**:193–200.

197. Anjana PK, Babu B, Shaijumon MM *et al.* Lithium-ion-based electrochemical energy storage in a layered vanadium formate coordination polymer. *ChemPlusChem* 2020;**85**:1137–44.
198. Sandu G, Ernould B, Rolland J *et al.* Mechanochemical synthesis of PEDOT:PSS hydrogels for aqueous formulation of Li-ion battery electrodes. *ACS Appl Mater Interfaces* 2017;**9**:34865–74.
199. Poizot P, Gaubicher J, Renault S *et al.* Opportunities and challenges for organic electrodes in electrochemical energy storage. *Chem Rev* 2020;**120**:6490–557.
200. Gottis S, Barres AL, Dolhem F *et al.* Voltage gain in lithiated enolate-based organic cathode materials by isomeric effect. *ACS Appl Mater Interfaces* 2014;**6**:10870–6.
201. Wang J, Liu X, Jia H *et al.* A high-voltage organic framework for high-performance Na- and K-ion batteries. *ACS Energy Lett* 2022;**7**:668–74.
202. Jia H, Quan T, Liu X *et al.* Core-shell nanostructured organic redox polymer cathodes with superior performance. *Nano Energy* 2019;**64**:103949.
203. Rupp R, Vlad A. On the reliability of sodium metal anodes: the influence of neglected parameters. *J Electrochem Soc* 2019; **166**:A3122–31.
204. Jouhara A, Dupré N, Gaillot A-C *et al.* Raising the redox potential in carboxyphenolate-based positive organic materials via cation substitution. *Nat Commun* 2018;**9**: 4401.
205. Lakraychi AE, Deunf E, Fahsi K *et al.* An air-stable lithiated cathode material based on a 1,4-benzenedisulfonate backbone for organic Li-ion batteries. *J Mater Chem A* 2018;**6**: 19182–9.
206. Sieuw L, Lakraychi AE, Rambabu D *et al.* Through-space charge modulation overriding substituent effect: rise of the redox potential at 3.35 V in a lithium–phenolate stereoelectronic isomer. *Chem Mater* 2020;**32**:9996–10006.
207. Rambabu D, Lakraychi AE, Wang J *et al.* An electrically conducting Li-ion metal–organic framework. *J Am Chem Soc* 2021;**143**:11641–50.
208. Zhu Q, Wang J, Liu X *et al.* Mixed anionic and cationic redox chemistry in a tetrathiomolybdate amorphous coordination framework. *Angew Chem Int Ed* 2020;**59**:16579–86.
209. Sieuw L, Ernould B, Gohy J-F *et al.* On the improved electrochemistry of hybrid conducting-redox polymer electrodes. *Sci Rep* 2017;**7**:4847.